Scientific Excellence • Resource Protection & Conservation • Benefits for Canadians
Excellence scientifique • Protection et conservation des ressources • Bénéfices aux Canadiens

Coastally Trapped Waves on The Labrador Shelf

J.F. Middleton and D.G. Wright

Physical and Chemical Sciences Branch
Scotia-Fundy Region
Department of Fisheries and Oceans

Bedford Institute of Oceanography
P.O. Box 1006
Dartmouth, Nova Scotia
Canada B2Y 4A2

June 1989

Canadian Technical Report of Hydrography and Ocean Sciences No. 116

Fisheries and Oceans : Pêches et Océans

Canada

Canadian Technical Report of Hydrography and Ocean Sciences

Technical reports contain scientific and technical information that contributes to existing knowledge but which is not normally appropriate for primary literature. The subject matter is related generally to programs and interests of the Ocean Science and Surveys (OSS) sector of the Department of Fisheries and Oceans.

Technical reports may be cited as full publications. The correct citation appears above the abstract of each report. Each report is abstracted in *Aquatic Sciences and Fisheries Abstracts* and indexed in the Department's annual index to scientific and technical publications.

Technical reports are produced regionally but are numbered nationally. Requests for individual reports will be filled by the issuing establishment listed on the front cover and title page. Out of stock reports will be supplied for a fee by commercial agents.

Regional and headquarters establishments of Ocean Science and Surveys ceased publication of their various report series as of December 1981. A complete listing of these publications is published in the *Canadian Journal of Fisheries and Aquatic Sciences*, Volume 39: Index to Publications 1982. The current series, which begins with report number 1, was initiated in January 1982.

Rapport technique canadien sur l'hydrographie et les sciences océaniques

Les rapports techniques contiennent des renseignements scientifiques et techniques qui constituent une contribution aux connaissances actuelles, mais qui ne sont pas normalement appropriés pour la publication dans un journal scientifique. Le sujet est généralement lié aux programmes et intérêts du service des Sciences et levés océaniques (SLO) du ministère des Pêches et des Océans.

Les rapports techniques peuvent être cités comme des publications complètes. Le titre exact paraît au-dessus du résumé de chaque rapport. Les rapports techniques sont résumés dans la revue *Résumés des sciences aquatiques et halieutiques*, et ils sont classés dans l'index annuel des publications scientifiques et techniques du Ministère.

Les rapports techniques sont produits à l'échelon régional, mais numérotés à l'échelon national. Les demandes de rapports seront satisfaites par l'établissement auteur dont le nom figure sur la couverture et la page du titre. Les rapports épuisés seront fournis contre rétribution par des agents commerciaux.

Les établissements des Sciences et levés océaniques dans les régions et à l'administration centrale ont cessé de publier leurs diverses séries de rapports en décembre 1981. Une liste complète de ces publications figure dans le volume 39, Index des publications 1982 du *Journal canadien des sciences halieutiques et aquatiques*. La série actuelle a commencé avec la publication du rapport numéro 1 en janvier 1982.

Canadian Technical Report of

Hydrography and Ocean Sciences No. 116

June 1989

COASTALLY TRAPPED WAVES ON THE LABRADOR SHELF

by

J.F. Middleton[1] and D.G. Wright[2]

[1]School of Mathematics
University of New South Wales
Kensington, N.S.W. 2033
Australia

[2]Physical and Chemical Sciences Branch
Scotia-Fundy Region
Department of Fisheries and Oceans

Bedford Institute of Oceanography
P.O. Box 1006
Dartmouth, Nova Scotia
Canada B2Y 4A2

90-05225/

Acknowledgements

Some of the bottom pressure data considered in this report was collected and provided to us by Graham Symonds and John Lazier. It is a pleasure to thank them. We are also grateful to Brian Petrie and John Lazier for helpful comments on an earlier draft. Meg Burhoe typed the various versions of the manuscript in her usual competent and patient manner. Financial support for this work was provided by the Federal Panel on Energy Research and Development.

©Minister of Supply and Services 1989
Cat. No. Fs97-18/116 E ISSN 0711-6764

Correct citation for this publication:

Middleton, J.F. and Wright, D.G. 1989. Coastally trapped waves on the Labrador Shelf. Can.Tech. Rep. Hydrogr. Ocean Sci. No. 116: vi + 76 pp.

ABSTRACT

Middleton, J.F. and Wright, D.G. 1989. Coastally trapped waves on the Labrador Shelf. Can.Tech. Rep. Hydrogr. Ocean Sci. No. 116: vi + 76 pp.

Bottom pressure data were obtained at 10 sites on the Labrador Shelf during 1985-86. The pressure signals are highly coherent in the longshore direction, although less so in the cross-shelf direction. Estimates of the buoyancy frequency were used to determine the cross-shelf structure of the first three coastally trapped wave (CTW) modes at Saglek and Nain Banks. The first and second modes were found to be nearly identical to those computed for a purely barotropic ocean in the 86 h band. At lower frequencies differences in mode 2 arise due to the stratification. The first three CTW mode structures were also computed for Hamilton Bank. In contrast to the above, discrepancies between the second mode computed for the stratified and barotropic cases arise in the 86 h rather than low frequency band. For the third mode at all banks, the cross-shelf scale of modal variability is of order the internal deformation radius, and the stratified results differ in all frequency bands from their barotropic counterparts.

Using an idealised topographic representation of the complex shelf bathymetry, both the stratified and barotropic mode 1 and 2 amplitudes were determined from the data, using the method of Haines, Thompson and Weins (1989). (Insufficient data was available to reasonably fit all three modes.) In nearly all cases the stratified modes provided the superior fit where discrepancies with the barotropic modes were apparent. The fitting technique was also extended so as to determine the gain and phase of each mode with respect to forcing by Hudson Bay atmospheric pressure.

Results at low frequencies (600 h) show the amplitudes of modes 1 and 2 to be highly coherent, of comparable amplitude and only weakly coherent with atmospheric pressure. The lag between modes 1 and 2 is around 180° and calculations suggest that these low frequency shelf modes result from the scattering of a first mode wave incident on the topographic jump at the Hudson Strait/Labrador Shelf boundary. Estimates of residual spectral energy and a comparison with the observed phase lag between sites shows that the variability in bottom pressure is due primarily to these two wave modes propagating freely down the shelf.

In the 86 h band, near the resonant frequency of the Hudson Bay system, mode 1 is found to be dominant as predicted using the analysis of Middleton (1988) and most coherent with atmospheric pressure. The gain and phase of this mode with respect to atmospheric pressure are also in reasonable agreement with the theoretical predictions of Wright *et al.* (1987).

Estimates of residual spectral energy and a comparison with observed phase lags between sites show that bottom pressure variability is not fully accounted for by the two free wave modes fitted. Results do suggest that the free waves identified in the 86 h band are an important feature of bottom pressure variability between Cape Chidley and Nain. However, further south at Hamilton Bank, the model fit is not as successful. Indeed, a direct fit of modal eigenfunctions to the data from Hamilton Bank alone results in a substantial increase in mode 2 amplitude over that found in the fit to all data. (Mode 1 is unchanged.) This increased energy is not found in a corresponding direct fit at Nain Bank.

We note that in the 86 h band, wind stress forcing may generate waves within the domain of the measurements (i.e., between Cape Chidley and Hamilton Bank). These locally forced motions are not accounted for in our fit to free wave modes and will act to reduce the goodness of fit. Also, mode scattering due to the rugged topography between Nain and Hamilton Banks will act to reduce the goodness of fit. These effects will be considered in future reports.

RÉSUMÉ

Middleton, J.F. and Wright, D.G. 1989. Coastally trapped waves on the Labrador Shelf. Can.Tech. Rep. Hydrogr. Ocean Sci. No. 116: vi + 76 pp.

Des données de pression de fond ont été obtenues à 10 sites du Plateau continental du Labrador en 1985-86. Les signaux de pression, très cohérents le long du plateau, le sont beaucoup moins transversalement à celui-ci. Des estimations de la fréquence de portance hydraulique ont servi à déterminer la structure, transversalement au plateau, des trois premiers modes de houle avec piégeage côtier (CTW) aux bancs de Saglek et de Nain. On a observé que le premier et le second modes étaient presque identiques à ceux calculés pour un ocean purement barotrope dans la bande 86 h. Aux fréquences plus basses, des différences causées par la stratification apparaissent dans le mode 2. Les trois premières structure modales CTW ont également été calculées pour le banc de Hamilton. Contrairement aux données ci-dessus, des aberrances apparaissent entre les seconds modes calculés pour les cas stratifiés et les cas barotropes dans la bande 86 h, plutôt que dans les bandes de fréquence plus basse. En ce qui concerne le troisième mode à tous les bancs, l'échelle, transversalement au plateau, de la variabilité modale est de l'ordre du rayon de déformation interne, et les résultats pour la stratification diffèrent, dans toutes les bandes de fréquence, des valeurs barotropes correspondantes.

Grâce à une représentation topographique idéalisée de la bathymétrie complexe du plateau, les amplitudes des modes 1 et 2, tant stratifiés que barotropes, ont été déterminées à partir des données et à l'aide de la méthode de Haines, Thompson et Weins (1989)(on ne possédait pas suffisamment de données pour pouvoir effectuer un lissage valable de chacun des trois modes). Dans presque tous les cas, les modes stratifiés permettaient un lissage supérieur là où apparaisaient des aberrances dans les modes barotropes. La technique du lissage a également été étendue de façon à pouvoir déterminer le gain et la phase de chaque mode relativement à la contrainte exercée par la pression atmosphérique de la Baie d'Hudson.

Les résultats aux basses fréquences (600 h) montrent que les amplitudes des modes 1 et 2 sont très cohérentes entre elles, d'amplitude comparable, mais faiblement cohérentes avec la pression atmosphérique. Le décalage entre les modes 1 et 2 est d'environ 180° et les calculs laissent supposer que ces modes basse fréquence caractéristiques du plateau sont le résultat de la dispersion d'une houle premier mode sur l'accident topographique constitué par la limite entre le détroit de Hudson et le plateau continental du Labrador. Les estimations de l'énergie spectrale résiduelle et une étude comparative faisant appel aux décalages de phase observés entre les sites montrent que la variabilité de la pression de fond est principalement due à ces deux modes de houle se propageant librement dans le plateau.

Dans la bande 86 h. près de la fréquence de résonance du système de la baie d'Hudson, le mode 1 se révèle dominant, comme l'analyse de Middleton (1989) permettait de le prévoir, et tout à fait cohérent avec la pression atmosphérique. Les gain et phase de ce mode relativement à la pression atmosphérique sont également en bonne corrélation avec les prévisions théoriques de Wright et coll. (1987).

Les estimations de l'énergie spectrale résiduelle et une étude comparative faisant appel aux décalages de phase observés entre les sites montrent que la variabilité de la pression de fond ne s'explique pas complètement par les deux modes de houles libres lissés. Les résultats laissent supposer que les houles libres caractérisées dans la bande 86 h repésentent une importante caractéristique de la variabilité de la pression de fond entre Cape Chidley et Nain. Mais, plus au sud dans le banc de Hamilton, le modèle est moins satisfaisant. En fait, un lissage direct des fonctions modales propres aux données provenant seulement du banc de Hamilton se traduit par une augmentation sensible de l'amplitude du mode 2, comparativement au résultat obtenu par lissage de toutes les données (le mode 1 reste inchangé). Cet accroissement d'énergie ne se retrouve pas après le lissage direct correspondant pour le banc de Nain.

Nous remarquons que, dans la bande 86 h, la contrainte éolienne peut produire des houles se situant dans l'intervalle de mesures (soit entre Cape Chidley et le banc de Hamilton). Ces mouvements dus à des contraintes locales n'interviennent pas dans notre lissage de modes de houles libres, et cela en diminue évidemment la précision. En outre, la dispersion modale due à la topographie accidentée entre les bancs de Hamilton et de Nain amoindrit elle aussi la précision du lissage. Ces effets seront examinés dans de futurs rapports.

TABLE OF CONTENTS

		Page
Acknowledgements		ii
Abstract/Résumé		iii
1.0	Introduction	1
2.0	The Data Set and Preliminary Analysis	3
3.0	The Coastally Trapped Wave Modes	6
4.0	The Mode Fitting Method and Evaluation	15
5.0	Results of a Fit to All 10 Gauges	23
6.0	Modal Fits at Nain and Hamilton Banks Separately	34
7.0	Discussion and Conclusions	37
References		39
Tables		43
Figures		45

1.0 INTRODUCTION

In this report we examine data from an array of bottom pressure gauges deployed over the Labrador Shelf in the summer of 1985 and left in place for a period of one year (see Fig. 1 for gauge locations). In the past, subsurface pressure data have proven to be useful in the study of wave motions over shelves. Indeed, Hamon's (1962, 1963) observations of propagating adjusted sea level variations on the east coast of Australia spurred the study of coastally trapped waves (CTW's). Initially, Robinson (1964) suggested that the propagating disturbances were the signature of coastally trapped waves generated by atmospheric pressure variations over the shelf. Later, Adams and Buchwald (1969) showed that windstress is actually the dominant forcing mechanism for these CTW's. Gill and Schumann (1974) noted that, at low frequencies, the alongshelf scale of variations greatly exceeds the corresponding cross-shelf scale and used this information to justify the longwave approximation, resulting in a simple and elegant theory for the response of a shelf to meteorological forcing. This theory, and extensions of it, have provided the framework with which most subsequent observations of coastal circulation have been described and interpreted.

The theory discussed above was developed under the assumption of negligible alongshore variations in shelf bathymetry. When this assumption is violated (as it always is on some scale) there will be some scattering of the coherent wave field. For example, Brink (1980) showed that an ensemble of small scale bumps with properties qualitatively consistent with those occurring on real shelves could result in damping of the coherent wave field comparable to that attributable to bottom friction. Scattering by larger scale alongshelf variations have been considered by numerous authors [(e.g., Wang (1980); Hsueh (1980); Davis (1983); Webster (1987); Wilkin and Chapman (1987); Middleton and Wright (1988)]. A common conclusion from these studies is that alongshelf changes over distances of the order of the shelf width or less do result in substantial scattering of the wave modes, with enhanced scattering for both higher frequency and higher cross-shelf mode number. This conclusion

holds with or without the longwave approximation which, when made, filters out the short waves which can carry energy backwards along the shelf.

An important limitation of all of the above studies is the neglect of stratification effects. Stratification, if sufficiently strong, may eliminate the short wave modes [Huthnance (1978); Chapman (1983)] seemingly lending some support to studies in which the longwave approximation is made as in these studies the short waves are eliminated at the outset. However, even with stratification sufficiently strong that backward propagation of energy is eliminated, theoretical studies [e.g., Brink (1986); Wilkin and Chapman (1988)] indicate that mode scattering will still occur although it will, of course, only scatter energy into forward propagating waves.

Previous observational programs aimed at the study of shelf circulation have generally been mounted on relatively smooth shelves, at least in part to minimize the above-noted complications associated with topographic irregularities. In general, the resulting observations have shown reasonable agreement with model predictions in which alongshelf topographic variations are simply neglected.

The present study is motivated by the desire to better understand the sub-inertial circulation over the Labrador Shelf. Previous studies in this area have demonstrated that both windstress over the shelf and atmospheric pressure variations over Hudson Bay are important forcing mechanisms for wave motions in this area (Wright *et al.*, 1987; Webster and Narayanan, 1988). Further, these studies indicate that variations of coastal sea level at Nain Bank and currents at two sites on Saglek and Nain Banks are consistent with the response being dominated by the first two coastally trapped wave modes, at least to the north of Nain Bank. However, as is evident from Fig. 1, this shelf has highly irregular bottom topography, with order one depth changes occurring over alongshelf scales shorter than the shelf width in several places. Mode scattering might certainly be anticipated, particularly in the region south of Nain Bank. Future studies will examine these data for evidence of such scattering but, as a first step, we examine the applicability of a very simple model which includes

stratification effects but excludes wave scattering, into either forward or backward propagating modes. As will become evident, this approach will help identify features of the data which, though not related to mode scattering, might otherwise be attributed to this process. Its limited success will also clearly motivate and guide the development of more sophisticated models.

2.0 THE DATA SET AND PRELIMINARY ANALYSIS

The positions of ten Anderaa (WLR5-2) bottom pressure gauges deployed on the Labrador Shelf in the summer of 1985 are shown in Fig. 1. As indicated, four were deployed at or near the coast and six offshore to form two lines across Nain and Hamilton Banks. The outermost gauges, 6 and 10 lie close to the 600 m isobath which approximately defines the axis of the Labrador Current. All gauges were set with a sampling rate of one hour and successfully retrieved in the summer of 1986. The positions, depths and start and finish times of the bottom pressure records are indicated in Table 1. After editing, around 292 days of coincident, continuous data were obtained.

Six hourly estimates of surface atmospheric pressure data were also obtained from AES for each of the Hudson Bay coastal towns of Coral Harbour, Moosonee, Inukjuak and Churchill. Following Wright *et al.* 1987, these data were spatially averaged so as to obtain a mean pressure signal most indicative of atmospheric forcing over Hudson Bay.

All hourly bottom pressure (BP) data were low pass filtered to remove tidal energy using a Cartwright filter with 129 weights and a high frequency cut off of 27.8 h. The averaged Hudson Bay pressure data were also low pass filtered using a top hat transfer function with a cut off of 28 h. A 10% cosine taper centered on this cut off was applied to the transfer function so as to avoid Gibbs phenomena in the time domain. Following filtering, all time series were decimated to 12-hour samples and then linearly interpolated to the nearest half Julian Day.

The resultant time series of demeaned atmospheric pressure and coastal BP are plotted in Fig. 2. A small amount of residual diurnal tide is evident in the BP time series but most striking is the evident coherence between the pressure variability at all coastal sites. Brownell Point, Site 1, and Hamilton Bank, Site 7, are separated by 807 km. The coherence of coastal BP with Hudson Bay atmospheric pressure (HBP) is also marked, particularly during the "summer" months when direct wind forcing is least. The BP signals are in fact most energetic during winter when wind forcing is greatest but the effect of wind on BP will be dealt with in a future report.

As a preliminary to mode fitting, estimates of the power spectrum at each site were obtained by first blocking the data into 50 day (100 cycle) strings with a 7% overlap. Each block was then detrended, demeaned and a 10% cosine taper applied to reduce leakage. The spectral quantities computed from the resultant 6 blocks were recoloured, averaged and finally smoothed with an average over 3 adjacent frequency bands. The longest period resolved is 600 h (25 days) the bandwidth is 2.5×10^{-3} cph and the effective number of degrees of freedom for cross spectral quantities was estimated at around 17.

The power spectra for HBP and coastal BP (Fig. 3), are generally quite red although the latter show a peak at around the 86 h period, where both wind stress and HBP forcing are expected to be significant. Typically, the peaks in coastal BP represent an rms variability of 3-4 mb. Note also that the maximum spectral energy is found at Hebron, Site 2, rather than Brownell, Site 1, which lies closer to Hudson Strait, the presumed geographical origin of a major portion of the CTW energy. A possible explanation for the reduced energy at Brownell is that CTW energy originating in the order 500 m deep Hudson Strait is initially steered along f/h contours (f is the Coriolis parameter and h depth) and thus the shelf break, leading to a coastal shadow zone as discussed by Middleton and Wright (1988). Apparently the shadow zone does not extend as far south as Hebron. Further down the shelf spectral energy decreases, at least in part due to friction. Across both Nain and Hamilton Banks, spectral energy decreases with increased distance offshore to about one-fifth to one-tenth of the coastal levels.

In addition, we note that the 85 h band peak manifested in the coastal spectra vanishes at the outermost sites 5 and 10.

Estimates of the coherence and phase between all BP time series were also obtained. For the coastal sites, the highest coherence levels relative to Nain were generally in the 600 and 86 h bands and near 0.92. For all periods longer than 60 h, coherences exceeded 0.79 which may be compared with a 95% significance level of 0.48, below which coherences are indistinguishable from zero. The phase of coastal BP relative to Nain is plotted in Fig. 4(a) for the 600, 240, 86 and 70 h bands. Only lags which are statistically significant at the 95% confidence level are shown. Apart from the 600 h band, the results consistently show that phase propagates down the shelf with the coast on the right, as expected for CTW's. In the 86 h band the phase variation is reasonably linear over the four sites and indicates a speed of around 19 m/s ($\sim fL$ with $L = 160$ km and $f = 1.2 \times 10^{-4} sec^{-1}$), suggestive of a strong mode 1 CTW influence. In the 600 h band, Hebron and Hamilton Bank lag Nain by 1° and 5° respectively. As will be shown these alongshelf lags are consistent with those obtained from a combination of first and second CTW modes.

Across both Nain and Hamilton Banks the coherences are somewhat lower than those between coastal gauges although again the 600, 240, 86 and 70 h bands each exhibit coherences of 0.7 or greater. Plotted in Figs. 5(a) and 6(a) are the phase lags with respect to the coast for each band. At the longest periods, the lag increases linearly across the shelf. At shorter periods, the coast may lead or lag offshore sites.

In addition to observations of BP, the summertime density field was also determined through three CTD sections made across Nain and Hamilton Banks during the deployment (Oct. 1985) and retrieval (Aug. 1986) periods. The estimates of potential temperature, salinity, density and buoyancy frequency, presented in Fig. 7, which are from a hydrographic section across Hamilton Bank during October 1985, are typical of the available observations. The relatively warm, salty Labrador Sea water is separated from the colder and fresher shelf water by a front at the shelf break: the Labrador Current associated with this

front can reach speeds of up to 50 cm/s at the surface, (Peterson, 1987). Considerable structure exists in the upper 50 m of the water column due to freshwater discharge, solar heating and possibly instabilities of the Labrador Current.

Estimates of buoyancy frequency were also made and show a decrease from around 2-3 cph at 100 m to less than 0.5 cph at depths of 400 m or greater. These estimates are smaller than typical values found on other shelves [e.g., for the east Australian shelf, N(100 m) ≃ 5.7 cph and N(400 m) ≃ 2.9 cph (see Church *et al.*, 1986)] and suggest the Labrador shelf to be relatively weakly stratified.

The CTD sections and buoyancy frequencies estimated in 1985-1986 are similar to those obtained from ten sections made across the shelf between Saglek and Hamilton Banks in the summer of 1980 (Fissel and Lemon, 1982). Indeed, as shown in Fig. 8, the shelf edge estimates of N obtained in 1985-1986 are only marginally larger than those obtained in 1980, represented by the solid curve which is a subjective "eye ball" fit to the data presented by Fissel *et al.* (1982). The limited data available for winter months [e.g., Lazier (1982), Fissel *et al.* (1988)] indicate that the density stratification is further reduced during this season, particularly in the near-surface layer.

3.0 THE COASTALLY TRAPPED WAVE MODES

Following Clarke (1977) and Brink (1982), we assume that BP variations may be expanded as a set of CTW modes

$$p(x, t) = \sum a_n F_n(x, z) \Phi_n(y) e^{-i\omega t} \tag{3.1}$$

where ω denotes frequency, a_n mode amplitude, and the origin of the coordinate system is located at Cape Chidley, the northern limit of the Labrador coast. Offshore position is given by x, and y is negative and increases in magnitude down the shelf. The cross-shelf modes $F_n(x,z)$ are determined by solution of an eigenvalue problem (Brink, 1982, equation (2.3)) and depend both on the shelf bathymetry and stratification.

3.1 Longshore Structure

In the absence of forcing, and neglecting any coupling between the modes due to friction, the longshelf structure of the CTW modes may be estimated from the damped wave equation

$$\frac{d\Phi_n}{dy} - [ik_n + \gamma_n]\Phi_n = 0 \tag{3.2}$$

where wavenumber k_n, is related to phase speed through $c_n = \omega/k_n$ and γ_n^{-1} is a frictional length scale (see Clarke and VanGorder, 1986). Necessary conditions for the inclusion of friction using this simplified approach, (Brink, 1982) are that the length and time scales of spin-down be much greater than the wavelength and period, $\gamma_n \ll k_n$ and $c_n/\gamma_n \ll \omega$. In addition, the wave equation (3.2) is formally only valid provided that the scale of longshore topographic variation is much larger than the shelf width. Solutions to (3.2) are then given by

$$\Phi_n(y) = exp\{\int_0^y iK_n(\zeta)d\zeta \tag{3.3}$$

where $K_n = k_n(y) - i\gamma_n(y)$ is weakly dependent on y by virtue of the changing bathymetry. The model solution (3.3) implies that there is no scattering of energy between modes and in the frictionless limit the net time-averaged energy flux for each mode is independent of alongshore position.

However, topographic variations on the Labrador shelf certainly occur on scales of order the shelf width or less between Nain and Hamilton Banks (Fig. 1). The model solution (3.3) is thus formally invalid and we might expect energy incident on this region to be scattered amongst modes that can exist at Hamilton Bank. Indeed, for a barotropic ocean model, Middleton and Wright (1988) have shown that topographic jumps in shelf depth act to retard the propagation of incident mode energy through scattering into both short and long waves. Where sufficiently strong stratification is present, short waves may not exist, (Chapman, 1983) although energy may still be scattered amongst the long waves.

For the purpose of this preliminary analysis however, we shall simply assume that the model solution (3.3) is valid and address the question of scattering through inspection of the model fit below. In addition, we assume that the shelf bathymetry can be modelled using the three profiles across Saglek, Nain and Hamilton Banks shown in Figs. 1 and 9: the latter two profiles running through the cross-shelf strings of BP gauges. In particular, the Saglek Bank topography is assumed to apply from Hudson Strait at $y=0$ to Hebron, $y_H=-274$ km, roughly half way between Cape Chidley and the Nain Bank array. In this region wave propagation is governed by

$$\phi_n(y) = exp[iK_n^{SB} y] \tag{3.4a}$$

where $K^{SB}=k^S-iY^S$ denotes the complex wavenumber appropriate to Saglek Bank. Between Hebron and Goose Bay, $y_G=-774$ km, the shelf bathymetry is modelled by that across Nain Bank and wave propagation given by

$$\phi_n(y) = \phi_n(y_H) exp[iK_n^{NB}(y-y_H)]. \} \tag{3.4b}$$

From Goose Bay, about 100 km upstream of the Hamilton Bank mooring line, $y=-950$ km, the bathymetry of the latter is assumed and

$$\phi_n(y) = \phi_n(y_G) exp[iK_n^{NB}(y-y_G)]. \} \tag{3.4c}$$

The model (3.4) above allows for damping and progressive changes in wave speed that should arise from the gross variations in the shelf bathymetry. In addition, the chosen bathymetry models that at each of the BP gauge sites. Thus, the cross shelf modal structures $F_n(x,z)$, (dependent on bathymetry) should be representative of those at each site. We note that while the changes in ϕ_n, c_n and F_n are crudely incorporated through abrupt changes across isolated sections, phases are continuous and amplitudes are chosen such that the energy flux carried by each mode is conserved across these sections.

3.2 Cross-Shelf Structure

To determine the eigenfunctions $F_n(x,z)$ and wavenumbers $K_n = k_n - iY_n$ we must first specify bottom friction and stratification. The frictional scale Y_n is determined as an integral of the eigenfunctions F_n and is proportional to $r = C_D U_{rms}$ where C_D is a drag coefficient, taken to be 1.5×10^{-3}, and U_{rms} is a typical near bottom current speed, (Brink, 1982). Observations of near bottom current, (Fissel and Lemon, 1982) suggest U_{rms} to be around 8 cm/s for the bank, saddle and trough regions of the shelf so that $r \simeq 1.2 \times 10^{-2}$ cm/s. We use this constant value in all results presented below unless stated otherwise. This is a rather crude parameterization of bottom stress, but results are not strongly dependent on this choice.

The formulation of the CTW problem given by Brink (1982) assumes that N is a function of depth only. For the Labrador shelf the buoyancy frequency estimates in Fig. 7d show this to be approximately so, except in regions near the surface and Labrador Current. The estimates of N(z) to be used below were taken from the solid curve in Fig. 8, to a depth of 400 m, below which N is approximated by a constant.

With the above estimates of r and N(z), and the shelf bathymetry in Fig. 9, the eigenfunctions F_n, phase speeds c_n and friction scale Y_n^{-1} were obtained using BIGLOAD2, from the suite of CTW programs made available by Brink and Chapman (1985). The boundary conditions used were that $u = 0$ at the coast, (where depth $h = 20$ m) and that $u_x = 0$ at $x = XMAX$, taken to be around 500 km offshore. The validity of results obtained using this boundary condition is discussed below.

As a check on the stability of the modal structures computed, mode 3 at Hamilton Bank was determined using both a 25 (horizontal) $\times$ 17 (vertical) and 33×17 grid at a period of 7.3 days (175 h). [Mode 3 was chosen for this test because its structure should be more sensitive to model resolution than modes 1 and 2.] A rigid lid was not imposed in either case and the spatial resolution in the two cases were 20 and 15 km, respectively. Results for bottom pressure $F_3(x, -h(x))$ (not shown) showed only very small differences in modal structure between these runs. The phase speed of 1.62 m/s obtained using the 25×17 grid is, however,

slightly larger than the value of 1.47 m/s obtained using the 33×17 grid. Results obtained by increasing XMAX to 528 km and N by 20% for the 33×17 grid were also examined. In both cases, the results again changed little suggesting the modal structures and phase speeds are stable and insensitive to small variations in N and XMAX. A similar analysis for Saglek Bank led to the same conclusions. To minimize inaccuracies the 33×17 grid is adopted below with XMAX = 495 km.

The first three stratified modal eigenfunctions, F_n, dispersion relations, $k_n = k_n(\omega)$, and friction scales, γ_n, were determined for each Bank (see Table 2), and the dispersion relations are presented in Fig. 10. Also plotted are the dispersion relations for modes 2 and 3, obtained for a purely barotropic ocean. The dispersion relation for mode 1 was essentially the same with or without stratification. The barotropic results were obtained using the Brink and Chapman programs and the realistic offshore boundary condition of exponential decay,

$$F_n(x) = F_n(XMAX)\, exp\,[-k_n(x - XMAX)], \tag{3.5}$$

expected in a flat, deep ocean. For Saglek and Nain Banks the barotropic dispersion relations for modes 1 and 2 are nearly identical to those for a stratified ocean while those for mode 3 indicate somewhat slower phase propagation. For Hamilton Bank, mode 2 travels somewhat slower in a barotropic ocean.

Each of the eigenfunctions determined was normalized such that

$$\delta_{nm} = \int_{-h(o)}^{0} F_n F_m |_{x=0} dz + \int_{0}^{XMAX} h_x F_n F_m |_{z=-h} dx \tag{3.6}$$

and results for bottom pressure across Saglek, Nain and Hamilton Banks are presented in Figs. 11 and 12 for the 175 and 77 h bands, respectively. Mode 1 results are not presented since for periods greater than 2 days the long wave condition is valid and results are essentially the same for each Bank: pressure decreases linearly from the coast to near zero at the shelf break.

It is apparent from Figs. 11 and 12 that there are quantitative differences between bottom pressure modal structures determined from the baroclinic and barotropic analyses. We shall see below that the success of our mode fitting attempt is reduced if we choose to restrict attention to the barotropic modes. The differences between these results is perhaps surprising as a low frequency criterion for the eigenfunctions to be strongly barotropic is (Clarke and Brink, 1985).

$$(N_s \alpha_s / f)^2 \ll 1, \tag{3.7}$$

where N_s and α_s denote the cross-shelf average of buoyancy frequency and topographic slope. For the three Banks considered here, $(N_s\alpha_s/f)^2$ is small and around 0.02 suggesting that the computed stratified and barotropic modes should be nearly identical. Indeed, it was found that the stratified modes were in fact strongly barotropic (see, for example, Fig. 13a) as suggested by the above criterion.

Since the baroclinic modes were calculated with $u_x = 0$ at the offshore boundary and the barotropic modes were calculated with the more realistic condition (3.5) it is natural to suspect that this is the source of the discrepancies. However, comparisons between the barotropic modes obtained using these two different conditions, at locations and frequencies where discrepancies occur, (see, for example, Fig. 13b) clearly demonstrate that this is not a major problem.

On examining Fig. 10, it is perhaps not surprising to find significant differences between barotropic and baroclinic mode shapes at low frequencies. After all, at low frequencies the difference between modes 2 and 3 is determined by a relatively small change in the eigenvalue, k. Indeed, this is also true at higher frequencies on Hamilton Bank where significant differences are again found. This observation does not, however, explain the apparent failure of the criterion (3.7), particularly at low frequencies.

The difference between low frequency mode structures actually appears to be due, at least in part, to a kinematic effect associated with the cross-isobath advection of water. To

clarify this, let us begin with the assumption that the modal structures are strongly barotropic. Then

$$p_x^{BC}(-h) = p_x^{BT}(-h), \tag{3.8}$$

where the superscripts denote estimates based on the baroclinic (BC) and barotropic (BT) analysis, respectively. Since we wish to interpret bottom pressure data in terms of dynamical modes, we must examine how the pressure varies along the bottom.

$$[p^{BC}(-h)]_x = p_x^{BC}(-h) - h_x p_z^{BC}(-h) \tag{3.9}$$

$$= p_x^{BT}(-h) + h_x \rho(-h) g \tag{3.10}$$

where we have used (3.8) and the hydrostatic approximation to obtain (3.10). Here, ρ(-h) is the bottom density perturbation associated with the wave motion. For harmonic time dependence (complex amplitudes proportional to $e^{-i\omega t}$), the linearized density equation,

$$\rho_t + w\rho_{oz} = 0, \tag{3.11}$$

leads to

$$\rho = \frac{i\rho_o N^2}{\omega g} w, \tag{3.12}$$

and using

$$w \approx -u h_x \qquad at \;\; z = -h \tag{3.13}$$

yields

$$\rho = -(i\rho_o N^2 h_x/\omega g)u. \tag{3.14}$$

Substituting (3.14) in (3.10) we obtain

$$[p^{BC}(-h)]_x - p_x^{BT}(-h) = (Na/f)^2 \rho_o f^2 (u(-h)/i\omega). \tag{3.15}$$

Finally, using

$$p_x^{BT}(-h) \sim \rho_w f v(-h).$$

we estimate the relative difference in pressure gradient, δ, as

$$\delta \sim -i(N\alpha/f)^2(f/\omega)u(-h)/v(-h).$$

Clearly, even if $(N\alpha/f)^2 \ll 1$, there can be significant differences in bottom pressure variations estimated with baroclinic and barotropic models. In particular, we expect larger differences at low frequencies and for higher order modes, where u/v may not be small. Note, also, that since u/v is generally small for mode 1, the insensitivity of mode 1 to the inclusion or exclusion of stratification effects is consistent with the above argument.

Based on the above discussion, it seems likely that the differences between baroclinic and barotropic mode shapes are due to a real physical effect and not due to numerical inaccuracies. However, uncertainties do remain in our modal structures whether or not stratification is included (due, for example, to the fact that N is not independent of horizontal position or time in reality and to the fact that the influence of the Labrador Current has been ignored - see discussion below). In light of these uncertainties and as a check on the sensitivity of results to our mode shape estimates, we shall elect to fit both the stratified and barotropic modes. For the stratified modes, the computing cost in determining each modal structure at each frequency and for all three Banks is large. Each iteration in the resonance technique used takes about two minutes on a VAX/780 computer. Therefore at frequencies below or above the lower and higher frequency bands in Table 2, the modes and phase speeds as determined will be assumed valid. Between these bands, the eigenfunctions and phase speeds will be obtained by linear interpolation in frequency space. Mode 1 is of course non-dispersive and identical in all bands considered.

In the barotropic case, the modes are quickly determined. The realistic decay condition is assumed and eigenfunctions were determined for each mode and bank at 11 bands between the 60 and 600 h periods of dominant spectral energy. Linear interpolation in

frequency space was then used to obtain the eigenfunction and phase speed for the relevant spectral bands.

3.3 The Effect of the Labrador Current

Before proceeding to examine modal fits to the data we should at least estimate the (neglected) influence that the Labrador Current would have. A mean longshore current can change phase speeds of CTWs through advection and more importantly, change modal structure, through cross-shelf shear which acts to modify the mean potential vorticity, (see Narayanan and Webster, 1987, 1988). Here a simple model for the Labrador Current was obtained using time and depth averaged estimates of along isobath velocity obtained from current measurements made by the Bedford Institute of Oceanography across both Hamilton and Nain Banks. The mooring sites are indicated in Fig. 9.

The depth-averaged currents across Hamilton Bank, were used to crudely estimate the longshore current shown in Fig. 9c. The depth-independent model current linearly decreases from 11 cm/s at $x = 256$ km to zero at 335 km resulting in a net transport of 40 Sverdrups which is of order that inferred elsewhere, (Thompson *et al.*, 1986). With this transport, the mean current at Nain was estimated assuming the maximum to lie over the 600 m isobath, (Fig. 9b). The mean current at Saglek Bank was simply taken to be identical to that at Nain Bank.

From these current estimates, the first and second barotropic CTW modes and phase speeds were determined using the program BTCSW (Brink and Chapman, 1985) for several periods between 600 and 60 h. For Nain and Saglek Banks the modal results obtained were nearly identical to those determined in the absence of a longshore current. For Hamilton Bank the only significant effect of the longshore current was in mode 2 and for periods more than about 86 h. The effect of the mean current here is to increase phase speed by about 10% and respectively decrease (increase) the eigenfunction amplitude over the marginal trough (shelf) by about 25%.

Accounting for these differences had almost no effect on the results to be discussed below. While these results strictly apply only to the barotropic eigenfunctions (Brink and Chapman's programs do not allow for a mean current in the stratified case), they do at least suggest that the Labrador Current has little effect on the CTW modes. The influence of the Labrador Current is hence neglected in all results presented in the following sections.

4.0 THE MODE FITTING METHOD AND EVALUATION

The model for bottom pressure, p_i, at the i^{th} gauge site, x_i, is described by the linear equation

$$p_i = \sum_{j=1}^{m} E_{ij} a_j + \varepsilon_i, \tag{4.1}$$

where a_j denotes the j^{th} modal amplitude, ε_i a residual error and

$$E_{ij} = F_j(x_i, -h)\Phi_j(y_i)e^{-i\omega t}, \tag{4.2}$$

the CTW modal structures for bottom pressure. The Φ_j are given by equations (3.4) and the F_j are those barotropic or stratified modes obtained through the procedure described above. Note that the a_j are complex numbers which determine both the magnitude and the phase of the wave modes.

Rather than seek to determine the a_j for individual realizations we shall seek to determine the amplitude matrix

$$A = \langle a a^H \rangle \tag{4.3}$$

where the brackets $\langle\ \rangle$ denote the ensemble average, obtained by block and band averaging as discussed in section 2, and H denotes the transpose of the complex conjugate. The a may thus be complex and (4.3) will yield information regarding the coherence and phase lag between wave modes.

4.1 The Fitting Technique

The method used is due to Haines, Thompson and Weins (1989) and following these authors we post multiply (4.1) by the vector of bottom pressure, p^H, to obtain

$$P = P_M + <\varepsilon\varepsilon^H>, \tag{4.4}$$

where $P(\omega) = <pp^H>$ denotes the cross spectral matrix of observed bottom pressure at frequency ω and

$$P_M = EAE^H \tag{4.5}$$

is the model cross spectral matrix to be fitted to P. This fit is accomplished by minimising the error between model and observed cross spectral pressure matrices,

$$Q = \sum_j \sum_i (P - P_M)_{ij} (P^H - P_M^H)_{ij}, \tag{4.6}$$

with respect to the elements of A. After some algebra, Haines *et al.* (1989) have shown that the matrix of modal amplitudes is given by

$$A = KPK^H, \tag{4.7}$$

where $K = (E^HE)^{-1}E^H$. Note that the result may also be obtained by minimising $\varepsilon^H\varepsilon$ in (4.1) with respect to the a_j and then ensemble averaging.

The simplicity of the result (4.7) is remarkable and one consequence is that the degrees of freedom that pertain to P may be used to determine confidence intervals for the amplitude matrix A. Further, the cross spectral matrix P need only be determined once for each frequency so that a variety of models may be fitted with relative numerical ease. For example, fitting 3 modes implies that E^HE is a 3×3 matrix, the inversion of which is straightforward.

A further feature of the method described by Haines *et al.* is that the residual error is given by

$$R = P + P_M - EKP - PK^HE^H. \tag{4.8}$$

and will be positive semi-definite if P is, implying that the residual eigenvalues and residual energy are all positive. Note that it is for this reason that only coincident time series of pressure were used since it is only then that P is guaranteed to be positive semi-definite.

4.2 Model Evaluation

With the model amplitudes determined in principle by (4.6), the question of goodness of fit arises. Haines *et al.* (1989) point out that no adequate theory is yet available to evaluate the statistic Q as a measure of model validity. However, as a crude guide to goodness of fit it will be determined below.

A more objective method of evaluation, suggested by Haines *et al.*, is to see if the residual matrix R is consistent with uncorrelated random noise across the array. If so then the model represents a consistent description of the observations, although perhaps not unique. If the residual matrix is inconsistent with random noise then some unmodelled physics may remain. To test this hypothesis each element of a cross spectral matrix of noise R_e was determined as an average of 17 realizations (the number of degrees of freedom) of the cross spectral elements $Z_n Z_\ell^*$ where $Z_n = a_n + ib_n$ and a_n and b_n are selected from an N(0,1) random number generation for the $n = 1,10$ sites. With R_e so determined, the largest eigenvalue of R_e was obtained and normalized by the total variance of R_e. Repeating the process 200 times the statistical distribution of the largest eigenvalues was obtained and the 95% significance level determined at $\lambda_N = 0.28$. That is, if the residual signal is due solely to random noise, we expect that less than 28% of the variance in this residual would be associated with any single eigenmode of the residual matrix in 95 out of 100 realizations. Thus, if the normalized largest eigenvalue of the residual matrix exceeds this level, we conclude to 95% certainty that it is not drawn from an array of uncorrelated residual noise. While this single test will be applied to each frequency band, we note also that inspection of the matrix R_e may also reveal sites where the model fit is inadequate.

A second feature of model evaluation is the determination of the optimal number of modes that may be fitted to data from the array. Even in the absence of other oceanographic processes, we do not expect to be able to fit 10 CTW modes to the data from the 10 gauge sites, since the modes are not mutually orthogonal over the array. To examine this idea, consider the matrix

$$S = E^H E, \tag{4.9}$$

which is a direct measure of modal orthogonality over the array. For example, if

$$e_1 = \begin{pmatrix} 0 \\ 1 \end{pmatrix}, \quad e_2 = \frac{1}{\Delta}\begin{pmatrix} 1-e \\ e \end{pmatrix},$$

denote two modes, as measured at two sites, and $\Delta^2 = [1\text{-}e]^2 + e^2$, then $E = (e_1, e_2)$ and

$$S = \begin{pmatrix} 1 & e/\Delta \\ e/\Delta & 1 \end{pmatrix}.$$

Thus if e is zero, the modes are orthogonal and well resolved since mode 1 is measured only at site 2 and mode 2 only at site 1. As e tends to unity, the modes, as measured, become indistinguishable, S becomes ill-conditioned and from (4.6) the amplitude matrix A cannot be determined.

Even where e is unequal to one, errors in the modal structures themselves may be sufficient to make their sensible resolution impossible. A simple criterion for such resolution may be stated in terms of the typical fractional error in the elements of S that can lead to ill-conditioning. From Noble (1969), the relative error which will lead to ill-conditioning is given by

$$\delta S/S = \{\sum\sum |S_{ij} S^{-1}_{ji}|\}^{-1}. \tag{4.10}$$

and for the example above is equal to $\frac{1}{2}(\Delta^2\text{-}e^2)(\Delta^2 + e^2)$. The typical fractional errors in E that will lead to ill-conditioning are one-half of (4.10) since from (4.9) $\delta E/E \sim \frac{1}{2}\delta S/S$. Thus as e vanishes and the measured modes are orthogonal, errors of $\pm\frac{1}{4}$ in E are sufficient to render S

ill-conditioned. As e approaches unity, $\delta E/E$ vanishes so that any error will lead to ill-conditioning.

Neglecting possible wave scattering, the principal sources of error are thought to arise from our estimates of the mode 2 and 3 eigenfunctions and phase speeds; mode one seems well determined. Using the discrepancy between the computed stratified and barotropic dispersion curves as a rough guide, in the high frequency band, we find errors of 5 and 30% for F_2 and F_3. Linearizing (4.2) results in

$$\delta E/E \sim |\delta F/F + i\delta k y| . \tag{4.11}$$

and taking y=-460 km (Nain) and the k_n given in Table 3.1, we obtain fractional errors of 19%, for mode 2 and 55% for mode three. These error estimates only pertain to each mode. In fitting modes 1 and 2 alone a typical error for the matrix E might be $(0 + 0.19)/2 = 0.09$ since mode one is well determined. For a model fit of all three modes, $\delta E/E = (0 + 0.19 + 0.55)/3 = 0.25$. At low frequencies the k_n seem well determined although there are discrepancies of order 50% or more between the mode 2 and 3 barotropic and stratified eigenfunctions. For both modes we will take 50% as an estimate for the fractional error, so that the final estimate for $\delta E/E$ is 0.25 for a two mode model and 0.33 for a 3 mode fit.

4.3 Modal Amplitudes and Hudson Bay Pressure Wright *et al.* (1987) have shown that atmospheric pressure variations over Hudson Bay generate coastally trapped waves which propagate down the shelf through our array of bottom pressure gauges. The analysis technique described above estimates the modal amplitudes over the shelf but does not attempt to relate these amplitudes to any forcing mechanism. The method may however be easily extended to determine the relationships between modal amplitudes and hypothesized forcing mechanisms.

To determine the relationship between each wave mode and atmospheric pressure, p_o, we include a dummy mode in (4.1) which has a spatial structure orthogonal to all other modes. Thus, we define

$$\tilde{E}=\begin{pmatrix} e_0 & 0 \\ 0 & E \end{pmatrix}. \tag{4.12}$$

as the new matrix of modal structures where $e_0 = p_0/a_0$ is the dummy mode for atmospheric pressure. Note that $(e_0, 0)$ is clearly orthogonal to $(0, E^{i)}$

The cross spectral matrix of both atmospheric and bottom pressure p is denoted by

$$\tilde{P}=\begin{pmatrix} <p_0 p_0^H> & <p_0 p^H> \\ <p_0^H p> & P \end{pmatrix} \tag{4.13}$$

and the components of the amplitude matrix are given by

$$\tilde{A}_{11}=<a_0 a_0^H>=<p_0 p_0^H>/e_0^2, \tag{4.14}$$

$$\tilde{A}_{12}=\tilde{A}_{21}^H=<a_0 a^H>$$

$$=<p_0 p^H>ES^{-1}/e_0 \tag{4.15}$$

and

$$\tilde{A}_{22}=A\,. \tag{4.16}$$

as before. Thus, with little extra computational effort the method of Haines *et al.* (1989) is extended so as to determine the coherence, gain and phase of each CTW mode amplitude with respect to forcing by atmospheric pressure. Note also that the new residual matrix is given by

$$\tilde{R}=\begin{pmatrix} 0 & 0^H \\ 0 & R \end{pmatrix} \tag{4.17}$$

since atmospheric pressure is defined as a single mode, orthogonal to all others and so cannot lead to increased error.

4.4 Weighting

The amplitude matrix is determined by minimizing (4.6), the error between the observed and model cross spectral matrices summed over all sites. However, since both the observed and modal pressure amplitudes are relatively small at the shelf edge, the fit here may be expected to be poor compared to that at the coast where amplitudes and numbers of sites are larger.

The relative importance of each site may be changed through weighting. We define W as a weight matrix such that $W_{ii} = w_i$ and $W_{ij} = 0$ for $i \neq j$. Then premultiplying (4.1) by W we obtain

$$p = Ea + e,$$

where $p_i = w_i p_i$, $e_i = w_i \varepsilon_i$, and $E_{ij} = w_i E_{ij}$. The quantity to be minimized is

$$Q = \sum \sum <\varepsilon\varepsilon^H>>_{ij} <e^H e>_{ij},$$

so that clearly the contribution to the modal fit by each site varies with w_i^2.

When quantities with different units (e.g., pressure and velocity) are to be used together in the determination of modal amplitudes it is desirable to weight each input so that its importance is appropriately represented in the fitting procedure. For example, if each element is believed to be equally important in the determination of modal amplitudes then it would be reasonable to weight each time series by its standard deviation. In the present case where all variables have the same units, we have chosen to weight equally all variables included in the fit.

The weights may also be used to effectively delete sites from the modal fit. For example, we will seek to determine the modal amplitudes using the bottom pressure data from Hamilton Bank alone. The choice of weights required is simply that w_i is unity except at the sites to be deleted where w_i vanishes. In this case, it is fairly straightforward to show that Q is equal to the Q defined by the formal deletion of the unwanted sites. In addition, the only non-zero terms of A and R are just those that would be obtained if the unwanted sites were

altogether excluded from the analysis. The advantage of this method of site deletion is that only one numerical program is needed to fit modes to any subset of the site data available.

In the following we shall determine the modal amplitudes using data from all ten sites. In section 6 however, the modal amplitudes will be determined using only the data at each of Nain and Hamilton Banks. In each case the modal amplitudes determined will contain information regarding CTWs that may originate from different forcing and geographical origins. For example, we expect that one set of CTWs will arise from the coastal flux through Hudson Strait that is driven by atmospheric pressure. A second set will correspond to those waves forced by the wind over the backward region, and CTW's will also be generated by the local stress.

In the fit to all data, the amplitudes determined will be "biased" towards those pressure or wind forced CTW's which are dominant over the entire array. Note that those CTW's which are due to local wind forcing will tend to be filtered out since this locally forced response will have a spatial structure quite different from that of free CTW's generated to the north and simply propagating by the array. If locally forced motions (i.e., motions generated by forcing within the region where measurements were collected) dominate the observations, one may want to explicitly include an appropriate forced wave mode in the analysis. In the present case we are particularly interested in examining the influence of atmospheric pressure variations over Hudson Bay – an external forcing mechanism. The importance of these atmospheric pressure variations in driving CTW's will be determined through estimates of its gain, coherence and phase with respect to each modal amplitude. The measures of goodness of fit, coherence and phase lags between modes will also provide indirect information regarding the importance and geographical origin of the wind forced CTW modes.

In the fit to data at Nain and Hamilton Banks alone no assumptions will be made regarding phase propagation and the amplitudes determined will also contain information regarding CTW's due to local wind forcing. The similarity or otherwise of these amplitudes with those obtained from the fit to all data should crudely indicate the importance of wind

forcing and scattering as well as provide some measure of the validity of the model for phase propagation assumed in the fit to all data.

5.0 RESULTS OF A FIT TO ALL TEN GAUGES

Three combinations of the CTW modes were fitted to all available bottom pressure data: Model 1, Mode 1 alone, Model 2, Modes 1 and 2 and Model 3, Modes 1, 2 and 3. Both the stratified and barotropic modes were fitted and the results for the three models will be indicated by SM1, BM1, SM2, BM2 and SM3, BM3.

Note that in fitting the stratified modes, the γ_n used were those determined at each frequency band through interpolation of the high and low frequency estimates presented in Table 2. In the barotropic case, the low frequency values were assumed valid at all frequency bands. Since the parameterization of friction in (3.2) is only valid at low frequencies and in the long wave limit, neither of these representations of friction is strictly correct. However, in all bands excepting the lowest 600 h band, the results were found to be insensitive to friction and indeed varied little if the λ_n were chosen to be identically zero. In the 600 h band, friction is strongest and the necessary conditions $k_n \gg \lambda_n$ and $\omega \ll c_n/\lambda_n$ for its inclusion through the adopted procedures only weakly satisfied for modes 2 and 3. However, reducing friction to zero led to variations in the fitted amplitudes of only 10-20%.

5.1 Goodness of Fit

As a crude test of the goodness of fit, the fraction of variance

$$q(\omega) = \sum\sum P_{M_{ij}} / \sum\sum P_{ij} \tag{5.1}$$

that is accounted for by the model considered is presented in Fig. 14, along with the largest normalized eigenvalue $\lambda(\omega)$ of the residual matrix (4.8). The results for Model 1 in both the stratified and barotropic cases are nearly indistinguishable and as shown in Fig. 14 show a best fit in the 86 h band, where 85% of the variance is accounted for. The largest eigenvalue, λ,

of the residual matrix corresponding to this frequency band is 0.4. Thus, while 85% of the energy in this band is accounted for by our model, 40% of the residual energy is in a single eigenmode. Note that λ_N was determined as 0.28 at the 95% confidence level so that the residual matrix is inconsistent with uncorrelated noise. At periods other than 109 h, λ and q respectively increase and decrease suggesting that mode 1 alone is inadequate.

The addition of mode 2 does represent an improvement in both the explained variance and physics at low frequencies since q and λ respectively increase and decrease in these bands (Fig. 14). The stratified model SM2 is more successful than its barotropic counterpart BM2 at low frequencies although results for both are poor for periods of 60 h or less. Results for these higher frequency bands were obtained but will not be presented: there is, in fact, little energy in the observed pressures at these higher frequencies. The inclusion of a 3rd mode does not lead to any significant increase in explained variance and indeed its inclusion in both the stratified and barotropic models results in an increase in λ in most bands. Note that no results were obtained for BM3 at periods less than 86 h since the discrepancy between the 3rd stratified and barotropic modes were larger there and the latter is near its zero in group velocity for Nain and Saglek Banks.

The lack of improvement in goodness of fit for model 3 results is presumably due to the lack of orthogonality between modes 2 and 3. For both models SM3 and BM3 the fractional errors in E that will result in $S=E^HE$ being singular vary from only 3% in the 600 h band to 10% in the 60 h band. These are certainly less than our crudely estimated errors of 33 and 25% for the low and high frequency estimates of E given in section 4. For model 2, the tolerable errors in E are larger, varying from 10 to 16% between the 60 and 600 h bands. For these bands, the estimated errors in E are 25 and 9% so that modes 1 and 2 should be resolved at least at high frequencies and possibly at low frequencies in the baroclinic models since our error estimates may well be substantially overestimated in this case. Results for the three mode models will not however be presented.

The validity of the models fitted may also be examined through the residual matrix itself. In Fig. 15, the SM2 and BM2 model residual power at each site normalized by bottom pressure energy, $R_{ii}(\omega)/P_{ii}(\omega)$ is plotted against gauge site. Results for the SM2 model in the 600 h band show that the model error is less than 25% at all sites, except for those at the extreme edge of Nain and Hamilton Banks. Note, however, that at these locations the absolute energy levels are quite low so these large relative errors do not actually correspond to any increase in absolute error at the outer gauges. The mode 1 and 2 eigenfunctions are both very close to zero at these outermost sites so that larger relative errors may be expected. In addition, pressure at these sites may well be influenced by variability in the Labrador Current. While the fit in this low frequency band is otherwise reasonable, the residual errors in the 86 h band are much larger and the fit at the two outermost sites on Nain Bank is poor with errors of order 90%. At Hamilton Bank only the coastal energy is reasonably accounted for. The poorer fit in the 86 h band might be expected since any error in the idealized model for phase propagation will be amplified at higher frequencies where wavelengths are smaller. The 86 h band is also that for which wind forcing, and probably mode scattering, are greatest. The presence of locally forced motions and mode scattering between the measurement sites will also lead to an increase in error.

For the barotropic model BM2, the normalized error in the 86 h band is very similar to that in the stratified case. In this band the barotropic and stratified modes are near identical and as noted, the effect of friction is small. In the 600 h band, the barotropic residual errors are generally twice those found in the stratified case. The models here differ principally in the computed mode 2 eigenfunctions and frictional scale, λ_n^{-1}, at Nain, as shown in Fig. 11(b) and Table 2 (recall that the modes and phase speeds at frequencies below the lower value in Table 2 were approximated by the values in that band). A reduction of γ_n by a factor of 10 in the barotropic case (motivated by comparison of the baroclinic and barotropic results of Table 2) did not lead to an improved fit, suggesting that the low frequency stratified estimates of mode 2 are a closer representation of reality.

5.2 Free Waves

The amplitudes of modes 1 and 2 determined for each model are presented in Fig. 16 and in general mimic the amplitude of the bottom pressure spectra: larger energy is found at low frequencies with a shoulder near the 86 h band. For periods less than 109 h, the amplitudes of mode one obtained from each model are indistinguishable while the predicted mode 2 amplitudes are similar and about one-fifth of those for mode 1. In the 600 h band, the amplitudes of modes 1 and 2 predicted for the BM2 model are less than those obtained using the stratified modes. In both cases however, the amplitude of mode 2 is 50-85% of that for mode 1.

Note that the spectral estimates for modal amplitude $<a_j a_j^H>^{\frac{1}{2}}$ presented are related to those a_j in (3.1) by

$$a_j = (2\Delta\omega < a_j a_j^H >)^{\frac{1}{2}}.$$

where $\Delta\omega = 2.5 \times 10^{-3}$ cph. Thus, $a_j = 7.1 \times 10^{-2} < a_j a_j^H >^{\frac{1}{2}}$ with units mb·cm$^{1/2}$ or cm$^{3/2}$ if the units of pressure are taken as cm instead of mb. The corresponding mode amplitudes are in units of cm$^{1/2}$ [see (3.6), (4.1), (4.2), and Figs. 11-13]. Since the pressure and velocity fields are approximately barotropic, the latter can be simply obtained from geostrophy, $u = (g/f)\partial p/\partial x$, with pressure in cm. For mode 1 the results of SM2 indicate rms velocities of 4.9 and 1.7 cm/s for the 600 and 86 h bands. For mode 2 in the 600 h band the rms velocity within 30 km of the coast will be around 11 cm/s.

Clearly, mode 2 is important at low frequencies and as shown (Fig. 14), leads to a better goodness of fit in the stratified model. At higher frequencies mode 1 dominates and thus the similarity between model results for both amplitude and goodness of fit is expected.

The coherence between modes 1 and 2 (Fig. 17) is a maximum (0.90) in the 600 h band where amplitudes are largest. Both stratified and barotropic results are similar with mode 1 leading mode 2 by 160-170° for periods of 150 h or greater. In the 86 and 70 h bands the

coherencies are lowest and statistically indistinguishable from zero. (These results will be discussed below.)

As a further test of model 2 we compare the phase lags between predicted model pressure at each site (Figs. 4-6b) with those determined directly from the data (Figs. 4-6a). The predictions for phase are obtained directly from the cross spectral matrix of model pressure $P_M = E^H A E$ and those for SM2 are plotted in Figs. 4-6b for the coastal and bank gauge sites. For the coastal gauges (Fig. 4) the lags with respect to Nain show good agreement with the observations in the 600 h and 80 h bands. At other frequencies the agreement is only qualitative. Phase lags predicted by the barotropic model show no better agreement and are within a few degrees of the stratified results presented.

Across Nain Bank (Fig. 5) the agreement with observations at low frequencies is again reasonable. However, at higher frequencies the stratified and barotropic models both predict that the coast should increasingly lead the offshore, a result observed only at site 5. At sites 4 and 6, observations in both the 86 and 70 h bands show that these offshore pressures lead the coast. Again, the inadequacy of the model predictions may result from the neglect of local wind forcing, mode scattering, offshore influences, or errors in the phase propagation model assumed.

At the outer edge of Nain Bank, site 6, the model predictions suggest that the coast should lag or lead by around 180°. Such a result follows from the dominance of mode 1 and the fact that at the Bank edge it has an opposite sign to its coastal value. No improvement in predicted lag was found either at the Bank edge or inshore site through the addition of the third CTW mode in the model fit.

The predictions for Hamilton Bank (Fig. 6) are in qualitative agreement with the observed phase, in that the coast leads all offshore sites in the 600 and 240 h bands and lags in the 109-70 h bands. However, at low frequencies, the predicted phase leads are larger than observed while at higher frequencies the predicted lags are much less than observed. At the outermost gauge, site 10, the predicted lag in the 86 h band is near 180° again since mode 1 is

dominant and of opposite sign to its coastal value. The poor fit at Hamilton Bank is likely due in large part to the neglected influences of mode scattering and local forcing between Nain and Hamilton Banks. Also, the predicted longshore phase lags between these Banks (Fig. 4) are dominated by mode 1 in the 86 and 70 h bands but are larger than those observed, suggesting the possibility that a narrower shelf should have been assumed.

5.3 Hudson Bay Atmospheric Forcing

As pointed out earlier, the response to atmospheric forcing may be investigated since the gain, coherence and phase of each CTW mode may be immediately obtained from the first row or column of the amplitude matrix A. Before considering the modal response we examine the gain and phase of total coastal bottom pressure at Cape Chidley that is predicted by the model (3.1) and which may be written as

$$p(0,t) = p_0 \sum G_j e^{i\theta_j} F_j(0, -h(0)) e^{i\omega t}/e_0. \tag{5.2}$$

where G_j and θ_j denote the gain and phase of the jth CTW wave amplitude with respect to atmospheric pressure, $a_0 = p_0/e_0$. Results for the predicted Cape Chidley BP obtained using models SM1, BM1, SM2 and BM2 are very similar, (Figs. 18, 19) since the amplitude of mode 2 is both small and incoherent with atmospheric pressure in all frequency bands, (Fig. 20). (Results for SM1 and BM1 are not presented). Note that these estimates of gain and phase are based on the assumption that any additional forcing mechanisms are either dominated by or incoherent with atmospheric pressure variations over Hudson Bay. While this is a reasonable approximation near the ~85 h resonant period of the bay/strait system, away from this band windstress forcing may be both important and significantly correlated with the atmospheric pressure variations.

The theoretical predictions for gain and phase made by Wright *et al.* (1987, Fig. 5b, light curves) are also shown in Figs. 18 and 19. It is evident that best agreement is found in the 70-150 h band which includes the 85 h resonant period of the bay/strait system (Wright, *et*

al., 1987). In the low frequency band the agreement is poor. At these long time scales the response to pressure variations over Hudson Bay is weak and other effects likely dominate the coastal pressure.

As indicated, mode 2 is incoherent with atmospheric pressure in all bands and indeed results for the gain and phase of mode 1 (Figs. 21, 22) in all models are very similar to those for total pressure at Cape Chidley (cf. Figs. 18, 19). (These results are also little affected by the addition of mode 3). The dominance of the first mode in the forced response is also suggested by the analysis of Middleton (1988) who has detailed the generation of CTWs by an oscillatory coastal flux. In the present context the pressure difference across the mouth of Hudson Strait is approximately equal to the pressure at Cape Chidley (Wright *et al.*, 1987) so that from geostrophy, the coastal flux is $U(t) = p(0,t)/(2\ \rho\ f\ d)$, where $d = 100$ km denotes the half width of the strait. In the long-wave limit, the amplitude a_j of each CTW mode generated can be written as

$$a_j = p(0,t)h(0)b_j\, sinc(k_j d), \tag{5.3}$$

where

$$b_j = \frac{1}{h(0)} \int_{-h(0)}^{0} F_j(0,z)dz, \tag{5.4}$$

denotes the depth-averaged coastal pressure supported by the jth mode, h(0) refers to the depth of the strait (400 m) and $\mathrm{sinc}(x) \equiv \sin x/x$. Note the amplitudes a_j in (5.3) correspond to CTW's at $y = 0^+$ in the strait region of the shelf and we ignore for the moment the problem of how these CTWs are related to those on the shelf proper.

Estimates of b_j were obtained for Hudson Strait at a period of around 150 h at which the long-wave assumption is reasonably valid. The first two modal values obtained from the stratified analysis were 4.0×10^{-3} and 1.5×10^{-3} $cm^{-1/2}$ respectively, so that from 5.3 mode one should be dominant: the function sinc ($k_j d$) is near unity at low frequencies since $k_j d$ is small. However, as shown in Fig. 18, the pressure fluctuations at Cape Chidley that are driven by atmospheric forcing will be small at low frequencies. At higher frequencies the modes in

Hudson Strait are dispersive so that the long wave analysis of Middleton (1988) is no longer strictly valid. However, the result (5.3) may hold in a qualitative sense and for the resonant period of 85 h we obtain $b_1 = 3.6 \times 10^{-3}$, $b_2 = 0.9 \times 10^{-3}$ cm$^{-1/2}$ and sinc(k_jd) is equal to 1.0 and 0.54 for modes one and two respectively. These results suggest that the amplitude of mode 2 should be around 14% of that for mode 1 which is certainly consistent with the modal fit where $a_2 \simeq 0.15 a_1$.

5.4 Wave Scattering

In the above comparison we have assumed that the modal amplitudes in the Strait are equal to those on the shelf. However, the Strait is some 400 m deep and the boundary with the shelf represents an abrupt topographic jump which may well lead to scattering of energy between the CTW modes, (Middleton and Wright, 1988). It would thus be helpful to compare pressure variations just north of Cape Chidley ($y = 0^+$) with those to the south. While no observations of bottom pressure are available in the Strait region of the shelf, the discussion above does suggest that mode 1 is most efficiently generated by the oscillatory flux with an amplitude at $y = 0^+$ given by (5.3) as

$$a_1 = p_0 G e^{i\theta} h(0) b_1$$

or

$$a_1 / p_0 = 1.6 G e^{i\theta}. \tag{5.5}$$

The gain, G, and phase, θ, refer to the response of Cape Chidley pressure ($y = 0^+$) due to atmospheric pressure forcing, which we will estimate using the theoretical result derived by Wright *et al.* (1987) (see the broken lines in Figs. 18, 19). This gives an estimate of the coastal pressure associated with mode 1 at $y = 0^+$, which is based entirely on idealized theoretical models.

At $y = 0^-$ we can estimate the mode 1 amplitude associated with atmospheric pressure variations over Hudson Bay using the gain and phase of our mode 1 (estimated by the

modal fit to the data) on Hudson Bay pressure (see Figs. 21, 22). Thus south of Cape Chidley we have

$$a_1/p_0 = G_1 e^{i\theta_1}. \tag{5.6}$$

where the gain and phase are those between mode 1 on the shelf and Hudson Bay atmospheric pressure. Results for the phase, θ_1, are very similar to those presented in Fig. 19 (solid lines) and qualitatively similar to the predictions made by Wright *et al.* (1987). The predicted and estimated gain of mode 1, given by (5.5) [appropriate to $y=0^+$] and (5.6) [appropriate to $y=0^-$], are presented in Fig. 23.

In the resonant band 70-109 h, the predicted amplitude of mode 1 in the strait is around 1.5 of that estimated for the mode 1 CTW on the shelf. The net energy flux associated with each mode is

$$\Gamma_j = a_j^2/4\rho f. \tag{5.7}$$

Thus, the energy flux associated with our estimate of mode 1 on the shelf is only 4/9 of that associated with our estimate of mode 1 just inside the strait. If this is assumed to be a real energy loss [certainly a questionable assumption given the uncertainties in both model and statistical results used in deriving (5.5) and (5.6)], then it is reasonable to ask where the other 5/9 of the energy has gone. If all of this energy went into mode 2, then Γ_2 would equal 1.25 Γ_1 suggesting that $a_2 \approx 1.1a_1$. As noted however, the fitted amplitude of mode 2 is small; $a_2 \approx 0.15a_1$, suggesting either that (a) the predicted gain (5.5) from the analysis of Middleton (1988) and Wright *et al.* (1987) is too large, or (b) some energy is scattered offshore and into short reflected modes in the Strait. However, given the uncertainties in estimates based on (5.5) and (5.6), the qualitative consistencies between these results is indeed encouraging.

Unfortunately, no adequate theory yet exists for wave scattering at dispersive frequencies in either a barotropic or stratified ocean. At very low frequencies some progress has been made by Middleton and Wright (1988) and Johnson (1989). In their barotropic

analysis, Middleton and Wright (1988) have shown that a first mode CTW incident on an abrupt decrease in shelf depth will scatter energy into both long transmitted and short reflected modes. The result pertinent to the low frequency analysis here is that amongst the transmitted waves, the first two modes are dominant, of comparable amplitude and 180° out of phase. These features are generally consistent with our estimates for modal amplitudes (Fig. 16) and phase (Fig. 17) in the 600 h band and, at least in the 600 h band, modes 1 and 2 are highly coherent (0.90).

While the existence of short waves at low frequencies is questionable on the Labrador Shelf, the 180° lag between modes 1 and 2 can also be obtained from the scattering analysis of Johnson (1989). In that work, Johnson argues that a closer representation of scattering in a stratified ocean can be obtained by simply excluding the short waves so that at low frequencies, the streamfunction Ψ must be then approximately constant along continuous f/h contours. All of the incident energy is then transmitted across the jump though it may be scattered into different forward propagating wave modes. On either side of the topographic jump that divides Hudson Strait at $y=0^+$ from the shelf proper at $y=0^-$ we then have

$$\Psi(x^+)=\Psi(x^-) \tag{5.8}$$

where

$$x^-=x^-(h(x^+)),$$

and a one to one correspondence between x and h is assumed in each region. To illustrate the scattering theory, we choose to model the shelf regions on either side of the strait/shelf topographic jump by the exponential profiles

$$h=\left\{\begin{array}{ll} h_0^+ exp(2b^+x^+) & , y>0 \\ h_0^- exp(2b^-x^-) & , y<0 \end{array}\right\}. \tag{5.10}$$

so that

$$x^-=[b^+x^+ + \tfrac{1}{2}\ell n(h_0^+/h_0^-)]/b^- . \tag{5.11}$$

With the parameters, $h_0^+ = 400$ m, $h_0^- = 200$ m, $b^+ = 0.66$ and $b^- = 1.01$, the L = 1500 m depth contour is independent of x and for simplicity we assume that Ψ vanishes there. The eigenfunctions are then

$$\Psi_n = a_n e^{bx} \sin(n\pi x/L). \tag{5.12}$$

and the corresponding net longshore energy flux is

$$\Gamma_n = a_n^2 \rho b f l / 4 h_0. \tag{5.13}$$

(see Middleton and Wright, 1988). The modal amplitudes a_n forward of the strait may then be calculated for an incident mode Ψ_I from the Fourier series

$$g(x^-) = \sum \Psi_n(x^-). \tag{5.14}$$

where

$$g(x^-) = \left\{ \begin{array}{ll} 0 & , \ 0 \le x^- \le L_0 \\ \Psi_I[x^+(h(x^-))] & , \ L_0 \le x^- \le L \end{array} \right\}. \tag{5.15}$$

where $L_0 = (2b^-)^{-1} \ell n(h_0^+/h_0^-) = 0.35L$ denotes the emergent position of the h_0^+ contour on the shelf at $y = 0^-$.

For a mode 1 incident wave the normalized amplitudes and energy fluxes of the first three transmitted waves are (0.46, -0.34, 0.01) and (0.63, 0.35, 0.0004). Again modes 1 and 2 are dominant accounting for 98% of the incident flux, of comparable magnitude and 180° out of phase. For a mode 2 incident wave the results are substantially different with amplitudes and fluxes of (0.15, 0.21, -0.47) and (0.07, 0.14, 0.66) so that mode 3 dominates and modes 1 and 2 are in phase. These results are perhaps of only qualitative interest since the exponential bathymetry is at best a crude representation of the actual shelf topography. They do suggest however, that the high coherence between modes 1 and 2 and the near 180° lags observed are due to the scattering of a mode 1 incident wave.

Finally, a possible alternative explanation for the observed lags of around 180° is that no scattering has taken place and that both modes have a common geographical origin at

either Davis or Denmark Straits. To test this hypothesis, typical shelf bathymetries on the Baffin and west Greenland coasts were used to compute first and second mode phase speeds of (15.6, 4.9) m/s and (5.9, 0.9) m/s respectively. A period of around 600 h was assumed for these barotropic calculations and the length of the Baffin and Greenland shelves estimated at 874 and 2109 km respectively. The resultant phase lags for the (600, 240, 150) h bands suggest that mode 1 should lead mode 2 by (-15, -39, -62)° and (160, -140, -79)° if Davis and Denmark Strait are respectively chosen as the geographical origin. In neither case does mode 1 lead by around 170° in all bands supporting the contention that the low frequency Labrador shelf modes result from the scattering of an incident mode 1 wave.

6.0 MODAL FITS AT NAIN AND HAMILTON BANKS SEPARATELY

In the above analysis, the modal amplitudes were determined by a fit to all data, with the assumed phase propagation between banks. Here we present results obtained by fitting the CTW models at just Nain Bank (sites 3-6) and Hamilton Bank (sites 7-10), respectively. Here, the models consist simply of the determined eigenfunctions at each Bank so that the fit is not constrained by assumptions regarding friction or phase propagation. In this case the amplitudes determined will contain more information from neglected effects, such as wind forcing, and through comparison with the results above, should highlight the importance of such effects. Note that for both Banks only the two mode barotropic and stratified models BM2 and SM2 will be considered.

6.1 The Fit at Nain Bank

Results for the measures of explained variance q and physics λ are presented in Fig. 24 for models SM2 and BM2. The explained variance is similar to that obtained in a fit to all data (Fig. 14a) except that in the highest frequency bands it is larger (~96%). The measure λ also peaks here indicating that more physics is unexplained than in the 86 h band. The estimates of λ are also generally larger than found in the fit to all data, although here they

should be compared with a value of $\lambda_N = 0.49$ that corresponds to a 4×4 residual noise matrix. Note also that the λ and q corresponding to the barotropic and stratified models are similar except at low frequencies where the former model again results in a poorer fit.

A further indicator of model fit is provided by the normalized residual R_{ii}/P_{ii} at each Bank site, (Fig. 25). Comparison with Fig. 15a shows a definite improvement in the fit at the inshore sites 3 and 4 for both models. Again the outermost sites are poorly represented by the models, notably BM2. In the 86 h band the residual variance is similar for both stratified and barotropic models since the computed eigenfunctions are nearly identical. In Fig. 5c the across shelf phase lags for the stratified model are close to those observed in the 240 and 600 h bands. Results for BM2, (not presented) on the other hand are in poor agreement with the observations. In the 70 and 86 h bands, both models show the coast to lag all sites, contrary to the consistent lead found in the fit to all data, Fig. 5b. However, both model lags between the two inshore sites agree well with the observed lags, where coherence is greatest, a result presumably forced by the larger spectral energy at these sites.

The modal amplitudes (Fig. 26) are similar to those found in the fit to all data, (Fig. 16). Modes 1 and 2 are of comparable magnitude in the 600 h band while at high frequencies the former is dominant. Again the barotropic model indicates a smaller mode 2 amplitude in the 600 h band where the goodness of fit is also poorer. The coherence (Fig. 27) between modes 1 and 2 for both models is high at both low and high frequencies with lags of around 170° and -135° respectively (Fig. 28).

The major improvement over the fit to all data lies in the better representation of cross shelf phase lag and spectral energy of each site. (Again the stratified model seems generally superior to that obtained using the barotropic modes, notably at low frequencies.) The better representation of cross shelf lag might be expected since no assumptions regarding alongshelf phase propagation are made here. The improved fit is achieved with only small changes to the estimated amplitudes of modes 1 and 2 obtained for the free wave model in the fit to all data. These results suggest that the estimated amplitudes at Nain are to a first

approximation those of free CTW's propagating from Hudson Strait. However, the poorer fit in the 86 h band does suggest that wind forcing is also important, and should be accounted for in the mode fitting exercise.

6.2 The Fit at Hamilton Bank

The explained variance q at Hamilton Bank (Fig. 29) again is larger than that obtained from a fit to all data. At low frequencies where the barotropic and stratified modes are most similar (in contrast with Nain Bank), the results for q and λ are most similar. At high frequencies the reverse holds and again the barotropic modes lead to a poorer fit. The estimates of R_{ii}/P_{ii} in Fig. 25 also show that the best fit is obtained for the stratified model and the residual variance is much reduced over that obtained in the fit to all data.

At low frequencies, the stratified model cross-shelf lags (Fig. 6(c)) are in excellent agreement with those observed. (The barotropic results are similar.) In the high frequency 70-86 h bands the model lags are in better agreement with those observed than found in the fit to all data. However, the lag between the inshore sites (7 and 8) are not as well modelled as at Nain and the normalized residual variance at site 8 is 24% which compares with 0.5% found for the equivalent site (4) at Nain. We note however that the "inshore" sites at Hamilton Bank are not as close to shore as those at Nain Bank. They actually straddle the marginal trough whereas the inshore sites at Nain Bank are both on the nearshore slope. This difference in positioning may partly explain the better fit at Nain Bank.

The improved fit for high frequencies at Hamilton Bank is achieved through a substantial change in the amplitude of mode 2 (compare Fig. 30 with Fig. 16) over that found in the fit to all data. (The amplitude of mode 1 is little changed except for the barotropic model at high frequencies where the fit is poor anyway.) The amplitude of mode 2 is now generally larger and around 3/5 of that for mode 1 at high frequencies. These high frequency results are not consistent with (unscattered) free wave propagation from Nain Bank to Hamilton Bank since the above clearly suggest an increase in the net energy flux carried by mode 2,

$\Gamma_2 = a_2^2/2\rho f$. Possibly the increased mode 2 energy is due to direct wind forcing between Nain and Hamilton Banks or cross shelf meanders of the Labrador Current may drive CTW's in a manner analogous to the coastal flux through Hudson Strait. It is also possible that some energy is scattered from mode 1 into mode 2 between Nain and Hamilton Banks. Some support for this possibility is found in the coherence between modes 1 and 2 at Hamilton Bank (Fig. 31). Further, where the coherence is largest the phase of mode 2 relative to mode 1 tends to be near 0 or 180° (Fig. 32) as expected if mode scattering were important If we simply assume that total energy carried by modes 1 and 2 is conserved between these two Banks, then

$$(a_1^{HB})^2 + (a_2^{HB})^2 = (a_1^{NB})^2 + (a_2^{NB})^2$$
$$\approx 1.04\,(a_1^{NB})^2$$

and if $a_2^{HB} = 3/5\, a_1^{HB}$, then

$$1.36(a_1^{HB})^2 = 1.04(a_1^{NB})^2$$
$$a_1^{HB} \approx 0.87 a_1^{NB}$$

so the large increase in a_2 between the two Banks (by a factor of 3) requires only a 13% decrease in mode 1. Clearly, we cannot conclude with any great confidence that the mode 1 amplitude has not decreased by this amount between these two locations. Thus mode scattering may well account for a significant increase in mode 2 between Nain and Hamilton Banks. On the other hand, physical arguments are easily made that there will be local wind forcing and an influence from the offshore between these Banks. Detailed examination of these effects will be the subject of future reports.

7.0 DISCUSSION AND CONCLUSIONS

Perhaps the most obvious conclusion from the work presented here is that deployment of an array of pressure gauges is a relatively inexpensive and effective means of obtaining information on the propagation of sub-inertial wave motions over large spatial scales. On the Labrador Shelf it was found that pressure records from sites separated by order

1000 km in the along-shore direction are strongly coherent, particularly for nearshore sites. Sites separated by order 100 km in the cross-shore direction are also quite strongly correlated but it is apparent that there are physical processes influencing the slope region which are not strongly felt near the coast, and vice versa. This is certainly not surprising given that the Labrador Current is well known to meander over the slope region (LeBlond, 1982) and that CTW's are after all coastally trapped.

The available data were sufficient to fit only two dynamical modes, but the results are very interesting. Before these data were analyzed, it had seemed possible (based on theoretical and numerical studies) that wave modes originating at or north of Cape Chidley might be so strongly scattered into different modes (both backward and forward propagating) that there might be no coherent signal reaching the Hamilton Bank line. This is certainly not true, at least for mode 1.

The mode fitting technique developed by Haines *et al.* (1989), and extended here so as to easily examine relations with assumed forcing terms, has proven to be a powerful and easily utilized tool. Indeed, the results presented here clearly show an improved fit to the data when baroclinic effects are included in the determination of modal characteristics. On the other hand, including the influence of the Labrador Current had very little influence. The ability to determine the better of two assumed models is encouraging and should be particularly useful in situations where opposing hypothesis (models) exist to explain some observations.

Low frequency results are consistent with the idea that the energy seen in mode 2 results from the scattering of mode 1 due to the topographic jump at Hudson Strait. At higher frequencies (period ~86 hr), where the influence of the Hudson Bay system is largest, mode 1 is clearly dominant, at least at Nain Bank, as predicted by the analysis of Middleton (1988). Further, mode 1 is most coherent with the atmospheric pressure variations over Hudson Bay in this band, and the gain and phase between these two series is in reasonable agreement with the predictions of Wright, *et al.* (1987).

However, bottom pressure variations over the Labrador Shelf are not fully accounted for by the model considered here. As already alluded to, the model does not do a good job of explaining pressure variations over the slope, presumably due to the influence of offshore current fluctuations not accounted for by our model. There is also evidence that the assumed physics between Nain and Hamilton Banks is a rather poor representation in the higher frequency band. In particular, a direct fit of modal amplitudes at Hamilton Bank alone shows a substantial increase in mode 2 amplitude compared to that estimated by a corresponding calculation at Nain Bank. This energy increase is inconsistent with the physics assumed in our model formulation. It suggests that energy is scattered from mode 1 into mode 2 between Nain Bank and Hamilton Bank, and/or local forcing by windstress or meanders in the Labrador Current is important in this region. These effects are being considered in ongoing research.

References

Adams, J.K. and V.T., Buchwald, 1969. The generation of continental shelf waves. J. Fluid Mech., 35(4), 815-826.

Brink, K.H., 1980. Propagation of barotropic continental shelf waves over irregular bottom topography. J. Phys. Oceanogr., 10, 765-778.

_____, 1982. The effect of bottom friction on low-frequency coastal trapped waves. J. Phys. Oceanogr., 12, 127-133.

_____, 1986. Scattering of long coastal-trapped waves due to bottom irregularities. Dyn. Atmos. Oceans, 10, 149-164.

_____ and D.C. Chapman, 1985. Programs for computing properties of coastal trapped waves and wind-forced motions over the continental shelf and slope. Tech. Rep. WHOI-85-17, 99 pp., Woods Hole Oceanogr. Inst., Woods Hole, MA.

Chapman, D.C., 1983. On the influence of stratification and continental shelf and slope topography on the dispersion of subinertial coastally trapped waves. J. Phys. Oceanogr., 13, 1641-1652.

Church, J.A., H.J. Freeland and R.L. Smith, 1986: Coastal-trapped waves on the east Australian continental shelf, Part I: Propagation of modes. J. Phys. Oceanogr., 16, 1929-1943.

Clarke, A.J., 1977. Observational and numerical evidence for wind-forced coastal trapped long waves. J. Phys. Oceanogr., I, 231-247.

_____ and K.H. Brink, 1985. The response of stratified frictional flow of slope and shelf waters to fluctuating large-scale, low-frequency wind forcing. J. Phys. Oceanogr., 15, 439-453.

_____ and S. Van Gorder, 1986: A method for estimating wind-driven, time-dependent, stratified shelf and slope water flow. J. Phys. Oceanogr., 16, 1013-1028.

Davis, A.M.J., 1983. Shelf similar topographies for free continental shelf waves. Geophys. Astrophys. Fluid Dyn., 23, 321-331.

Fissel, D.B. and D.D. Lemon, 1982. Analysis of oceanographic data from the Labrador Shelf, Summer 1980, vols. 1 and 2, Arctic Sciences Ltd., Sidney, British Columbia, Canada.

_____, G.J. Pierlot and O.J. Byrne, 1988: CTD measurements beneath the Labrador pack-ice: January-February, 1988. Arctic Sciences Ltd., Halifax, N.S., Canada.

Gill, A.E. and E.H. Schumann, 1974. The generation of long shelf waves by the wind. J. Phys. Oceanogr., 4, 83-90.

Haines, J., K.R. Thompson, and D. Weins, 1989. (Manuscript in preparation)

Hamon, B.V., 1962. The spectrum of mean sea level at Sydney, Coff's Harbour, and Lord Howe Island. J. Geophys. Res., 67, 5147-5155.

_____, 1963. Correction to "The spectrum of mean sea level at Sydney, Coff's Harbour, and Lord Howe Island." J. Geophys. Res., 69, 4635.

Hsueh, Y., 1980. Scattering of continental shelf waves by longshore variations in bottom topography. J. Geophys. Res., 85, 1147-1150.

Huthnance, J.M., 1978. On coastal trapped waves: Analysis and numerical calculations by inverse iteration. J. Phys. Oceanogr., 8, 74-92.

Johnson, E.R., 1989. (Manuscript in preparation).

Lazier, J.R.N., 1982. Seasonal variability of temperature and salinity in the Labrador Current. J. Mar. Res., 40, 341-356.

LeBlond, P.H., 1982. Satellite observations of Labrador Current undulations. Atmos.-Ocean, 20(2), 129-142.

Middleton, J.F. 1988. Longshelf waves generated by a coastal flux. J. Geophys. Res., 93(C9), 10724-10730.

_____ and D.G. Wright, 1988. Shelf wave scattering due to a longshore jump in topography. J. Phys. Oceanogr., 18(2), 230-242.

Narayanan, S. and I. Webster, 1987. Coastally trapped waves in the presence of a barotropic shelf edge jet. J. Geophys. Res., 92, 9494-9502.

_____ and_____, 1988. Coastally trapped waves in the presence of a shelf edge density front. J. Geophys. Res., 93(C11), 14025-14031.

Noble, 1969. Applied Linear Algebra. Apprentice Hall, N.J., 523 pp.

Peterson, I., 1987. A snapshot of the Labrador Current inferred from ice-flow movement in NOAA satellite imagery. Atmos.-Ocean, 25(4), 402-415.

Robinson, A.R., 1964. Continental shelf waves and the response of the sea level to weather systems. J. Geophys. Res., 69, 367-368.

Thompson, K.R., J.R.N. Lazier and B. Taylor, 1986. Wind-forced changes in Labrador Current transport. J. Geophys. Res., 91(C12), 14261-14268.

Wang, D.-P., 1980. Diffraction of continental shelf waves by irregular alongshore geometry. J. Phys. Oceanogr., 10, 1187-1199.

Webster, I., 1987. Scattering of coastally-trapped waves by changes in shelf width. J. Phys. Oceanogr., 17, 928-937.

_____ and S. Narayanan, 1988. Low-frequency current variability on the Labrador Shelf. J. Geophys. Res., 93(C7), 8163-8173.

Wilkin, J. and D.C. Chapman, 1987. Scattering of continental shelf waves at a discontinuity in shelf width. J. Phys. Oceanogr., 17, 713-724.

Wilkin, J. and D.C. Chapman, 1988. Scattering of coastal-trapped waves by irregularities in coastline and topography. EOS-Transactions of the American Geophysical Union, 69(44), 1277.

Wright, D.G., D.A. Greenberg and F.G. Majaess, 1987. The influence of bays on adjusted sea level over adjacent shelves with application to the Labrador Shelf. J. Geophys. Res., 92(C13), 14610-14620.

Table 1. Positions and record lengths of bottom pressure records at each site (see Fig. 1). Note that the depths of the WLR5-2 Aanderaa pressure gauges at the coastal sites 1-3 are indicated as 0m, although each was deployed under several meters of water. The record lengths and start times refer to the low pass filtered data.

Site Location	Site Number	Depth (m)	Lat °N	Long °W	Start Day/Month	Record Length (days)
Brownell	1	0	59.42	63.85	12/8	357
Hebron	2	0	58.18	62.62	12/8	357
Nain	3	0	56.55	61.68	11/8	357
Nain	4	204	56.55	60.32	18/10	292
Nain	5	175	56.95	59.27	17/10	292
Nain	6	571	57.05	58.96	17/10	292
Hamilton	7	109	53.63	55.75	7/7	390
Hamilton	8	145	53.84	55.18	7/7	390
Hamilton	9	200	53.73	52.61	6/7	390
Hamilton	10	600	54.01	52.86	6/7	390

Table 2. The stratified and barotropic phase speeds, c_n and frictional scales, γ_n, for the three topographic profiles. Note that in the barotropic case , the low frequency estimates of γ_n presented were used in all frequency bands..

	Mode	$\omega \times 10^2$cph	Stratified Modes		Barotropic Modes	
			C m sec^{-1}	$\gamma \times 10^3$ km^{-1}	C m sec^{-1}	$\gamma \times 10^3$ km^{-1}
S	1	–	12.83	0.08	12.45	0.08
A						
G	2	0.65	3.19	0.17	2.65	0.13
L		1.45	2.18	0.65	2.17	0.13
E	3	0.56	2.29	0.62	1.95	0.67
K		1.28	1.13	0.48	0.85	0.67
	1	–	13.4	0.06	13.0	0.07
N						
A	2	0.52	3.09	0.13	3.04	0.73
I		1.31	2.74	0.83	2.94	0.73
N	3	0.68	2.66	0.49	2.26	0.75
		1.15	1.97	0.11	1.35	0.75
H						
A	1	–	18.31	0.03	19.22	0.03
M						
I	2	0.60	2.31	0.12	2.01	0.13
L		1.25	1.80	0.14	1.41	0.13
T	3	0.56	1.47	0.80	1.45	0.91
O		1.36	1.26	0.95	1.28	0.91
N						

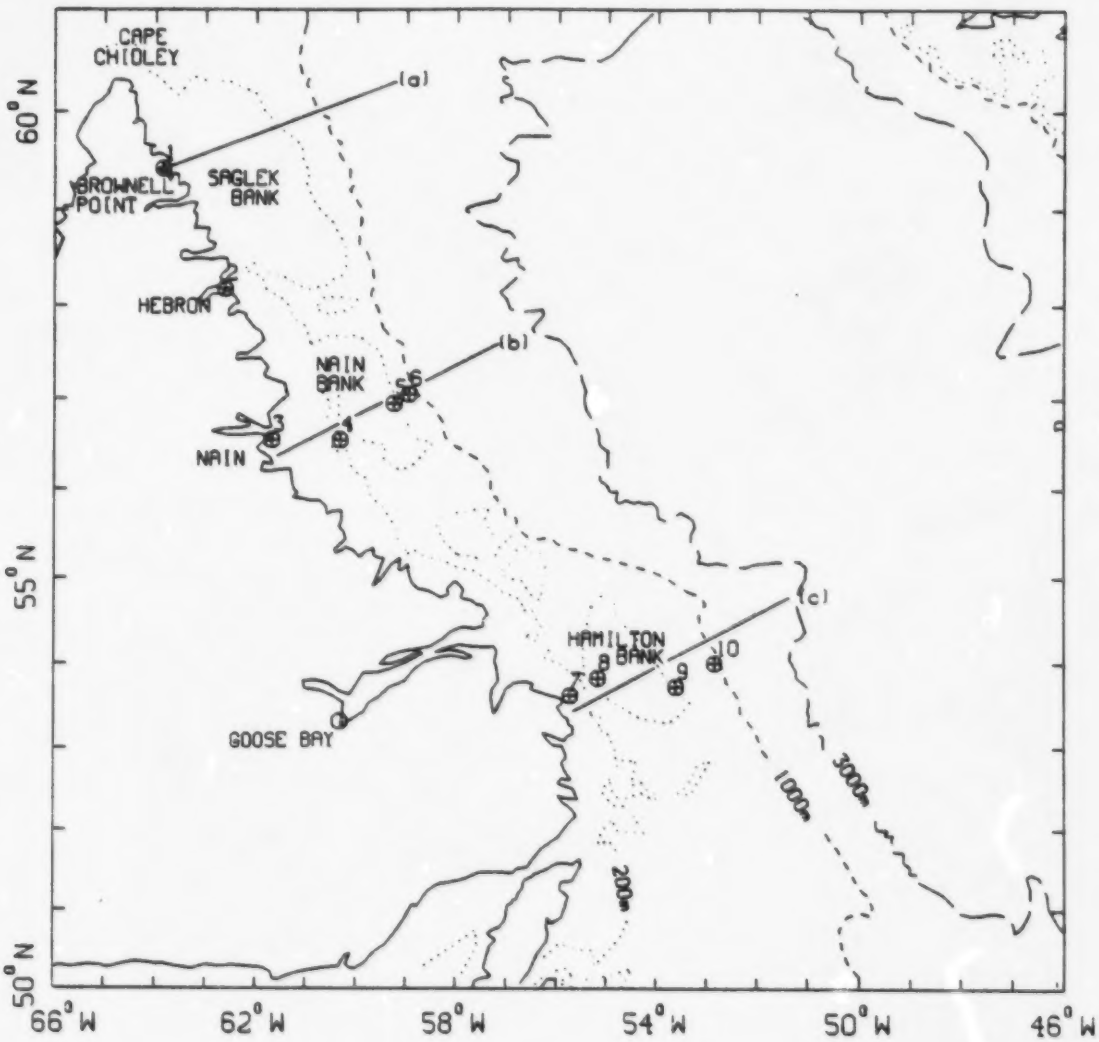

Fig. 1. The bathymetry of the Labrador Shelf. The bottom pressure gauge sites are indicated by the circles and the topographic sections (a), (b) and (c) are those used to compute eigenfunctions and phase speeds of the coastally trapped waves.

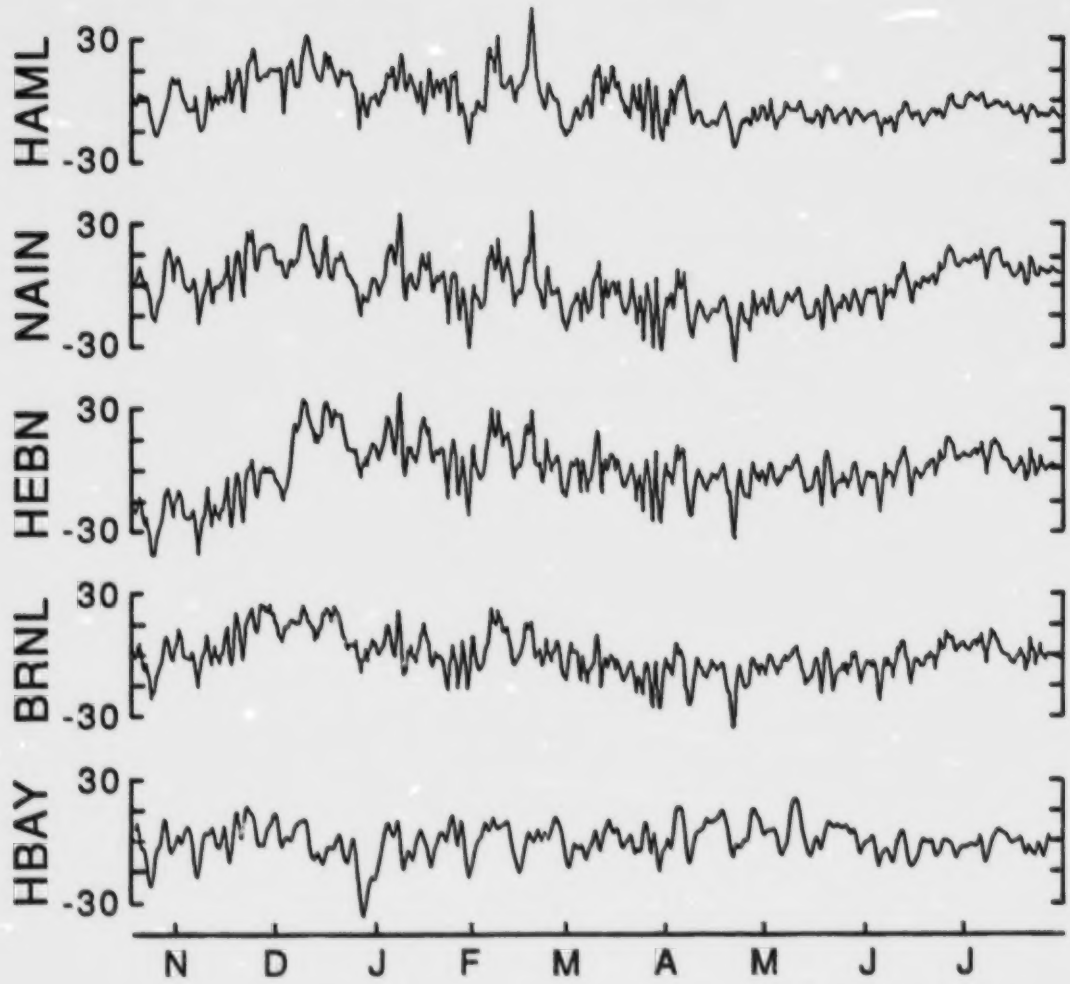

Fig. 2. Low pass filtered coastal bottom pressure at Brownell Point (BRNL), Hebron (HEBN), Nain and Hamilton Bank (HAML) [positions 1, 2, 3 and 7 on Fig. 1], and mean atmospheric pressure over Hudson Bay (HBAY). Units are millibars.

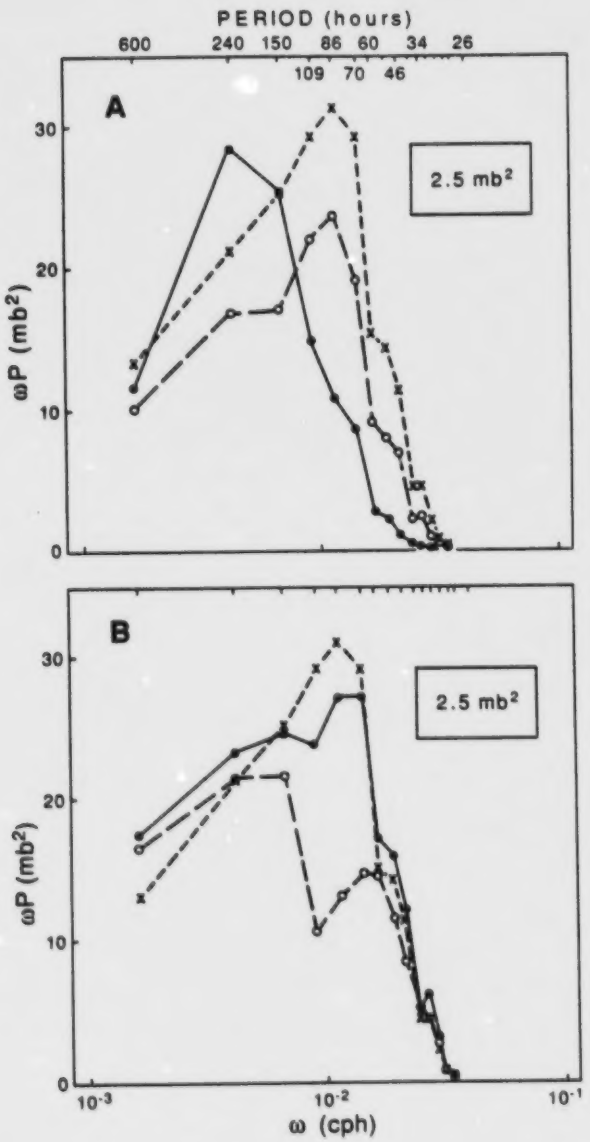

Fig. 3. (a) Autospectra of Hudson Bay atmospheric pressure (——), Brownell Point bottom pressure (—— ——) and Hebron bottom pressure (- - - -).

(b) Autospectra of Hebron bottom pressure (- - - -), Nain bottom pressure (——) and Hamilton Bank [site 7 on Fig. 1] bottom pressure(—— ——).

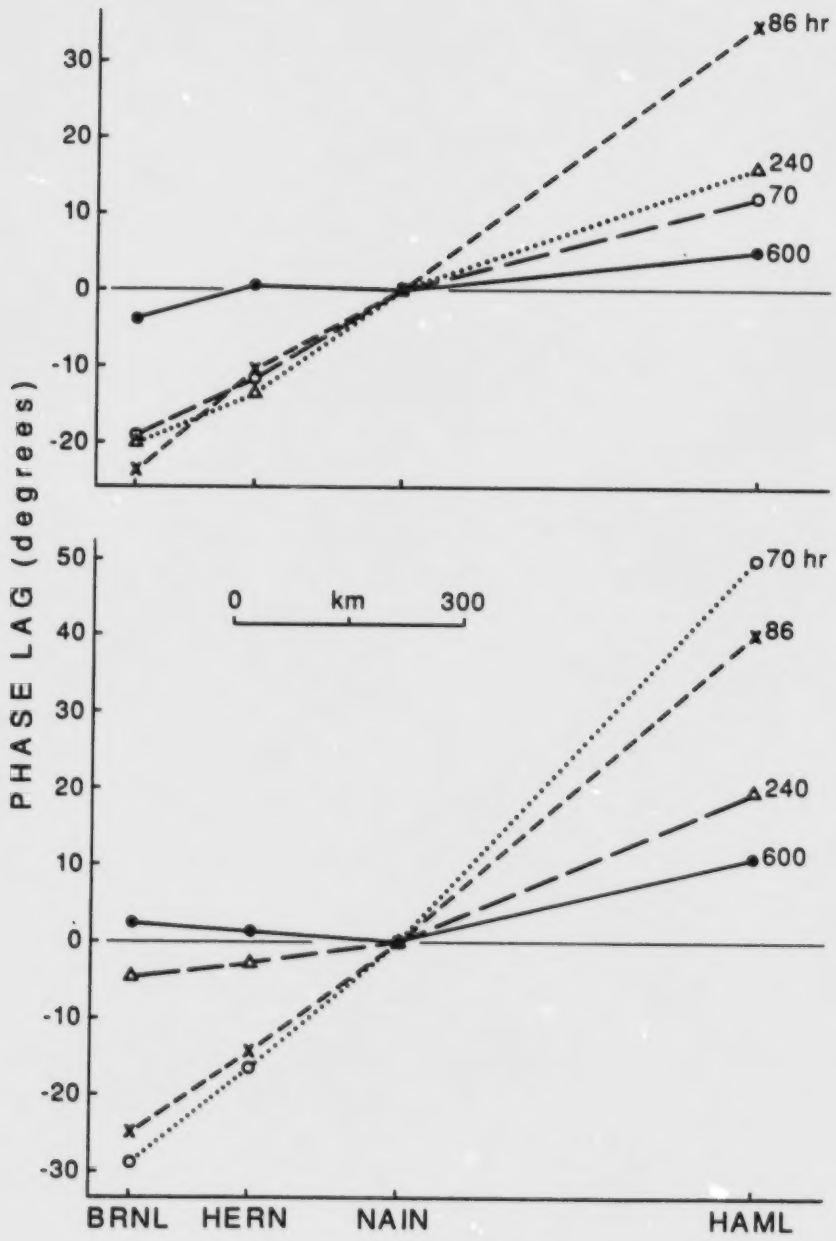

Fig. 4. (a) Along-shelf phase lag of observed coastal bottom pressure with respect to Nain for the 600,240,86 and 70 h bands. A positive phase means Nain leads. (b) The predicted lag of coastal bottom pressure with respect to Nain obtained using the fit of first and second stratified modes to the data (model SM2).

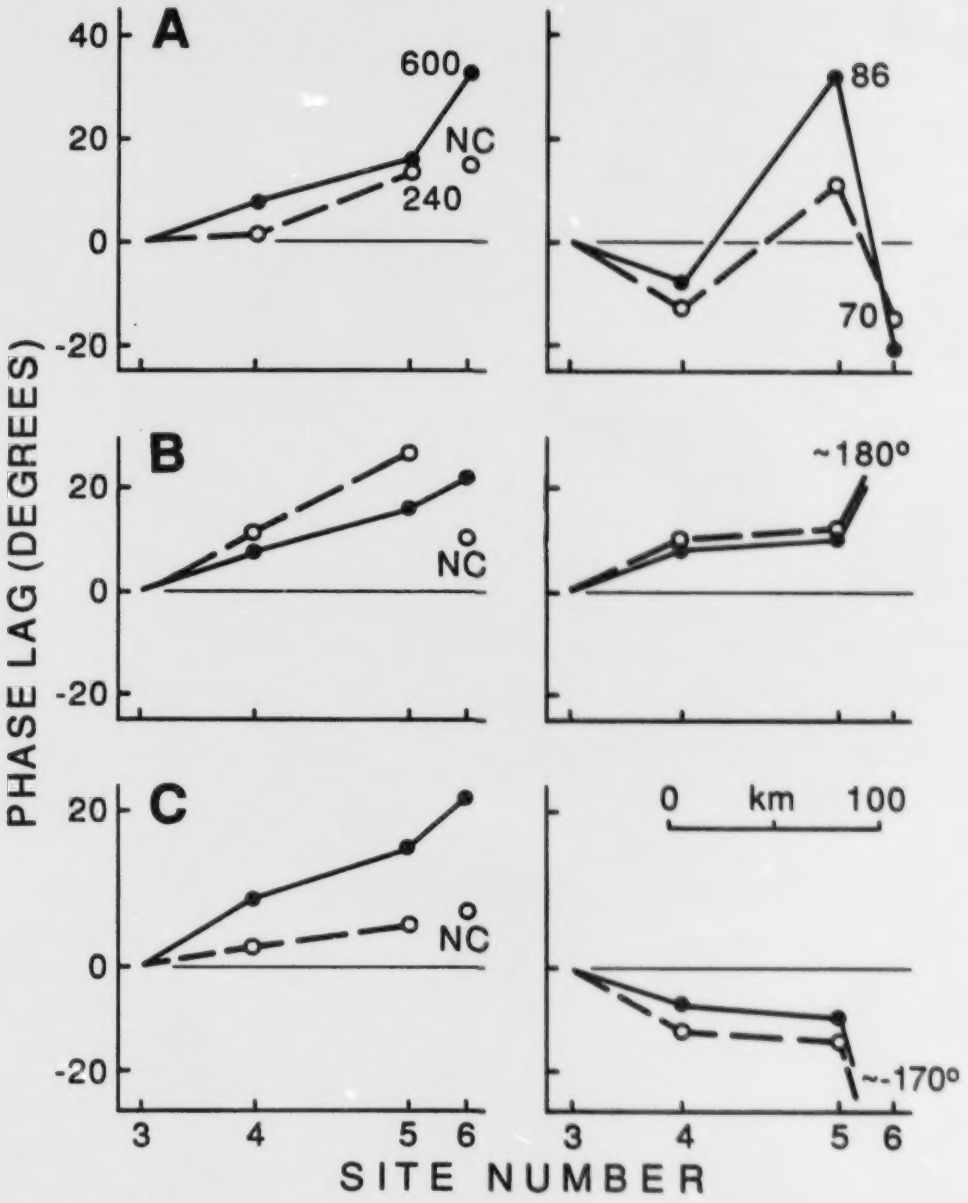

Fig. 5. (a) Phase lag of observed bottom pressure across Nain Bank with respect to the coast for the 600,240,86 and 70 h bands. A positive phase means the coast leads. (b) The predicted lags across Nain Bank obtained from a fit of the first and second stratified modes to all the data (model SM2). (c) The predicted lags obtained from model SM2 using only the Nain Bank data. Note that a value of nc indicates that the coherence is not distinguishable from zero at the 95% confidence level so that the lag error is ±180°.

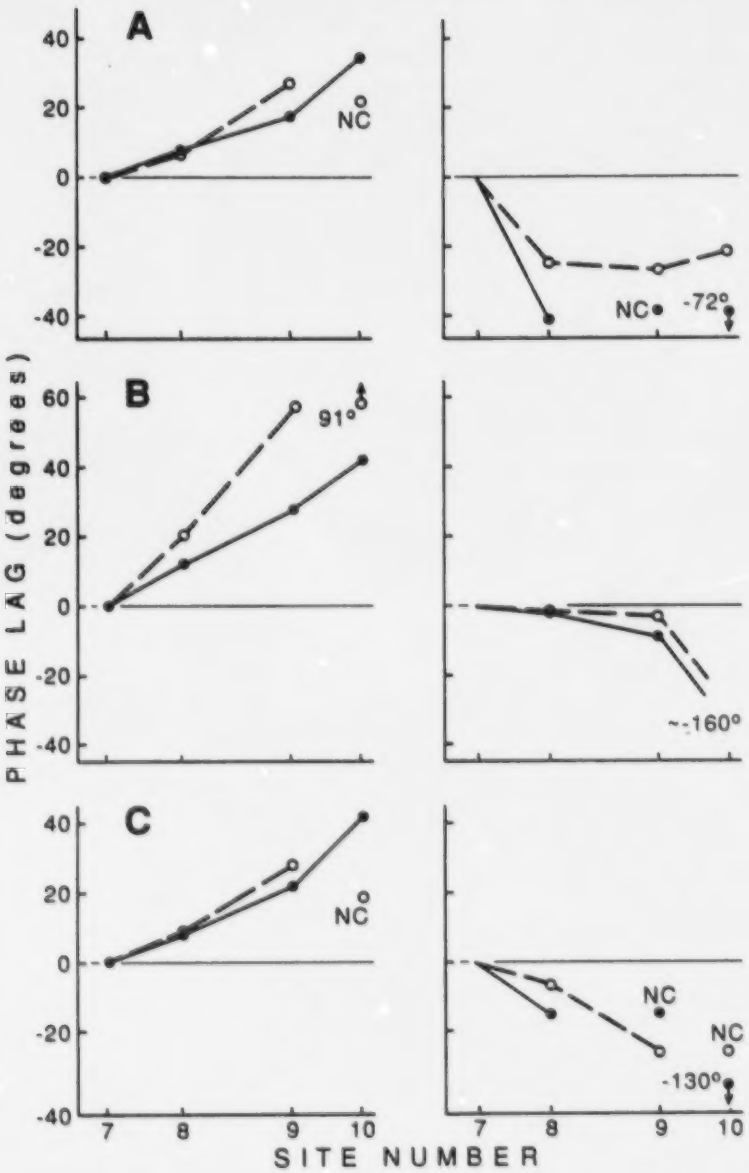

Fig. 6. As in Fig. 5 except the observed lags (a) and predicted lags (b) and (c) are for Hamilton Bank.

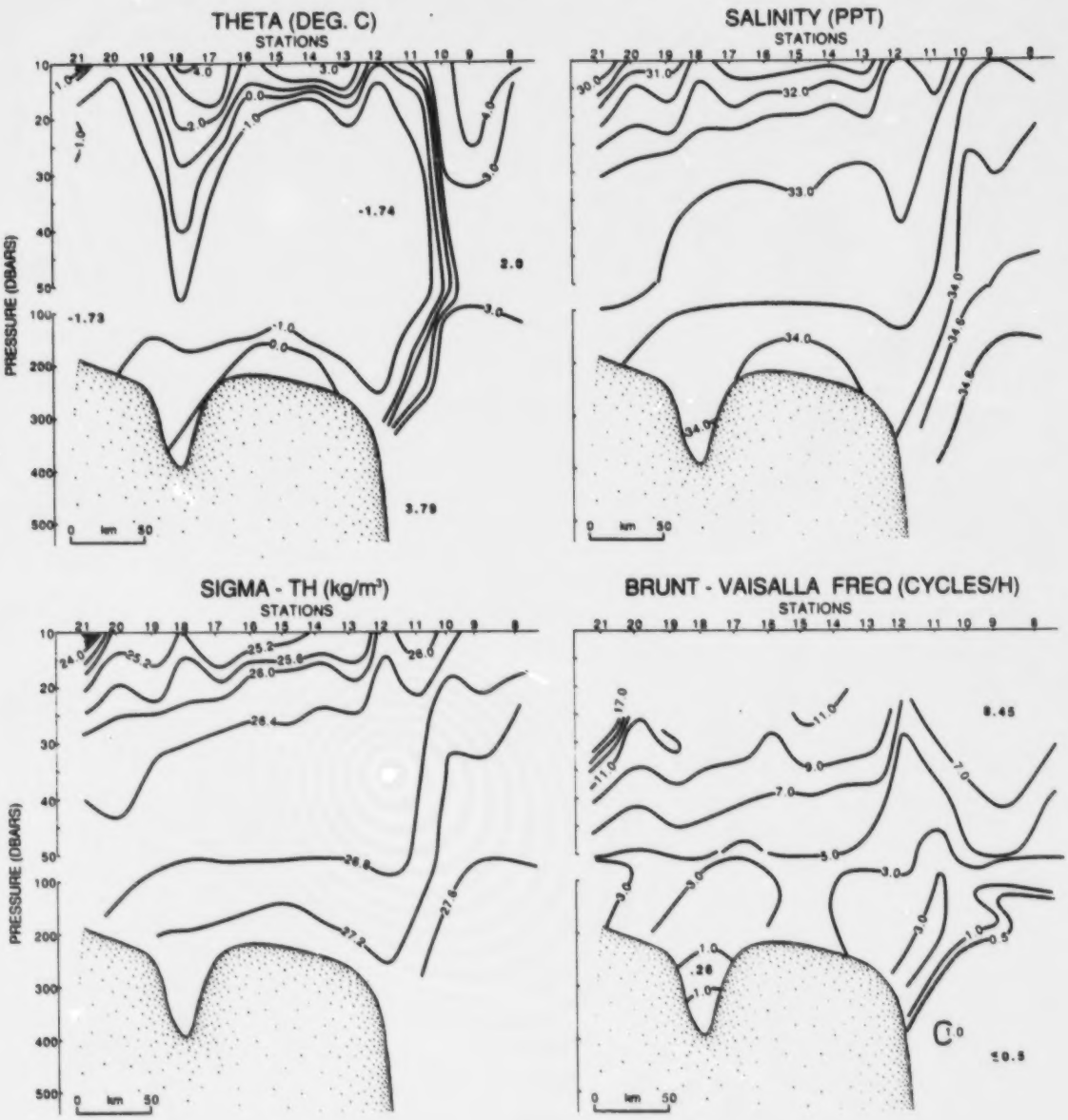

Fig. 7. **Results of a CTD survey across Hamilton Bank (Section (c) in Fig. 1), conducted during October 1985. Note that the vertical scale changes at a depth of 50 db.**

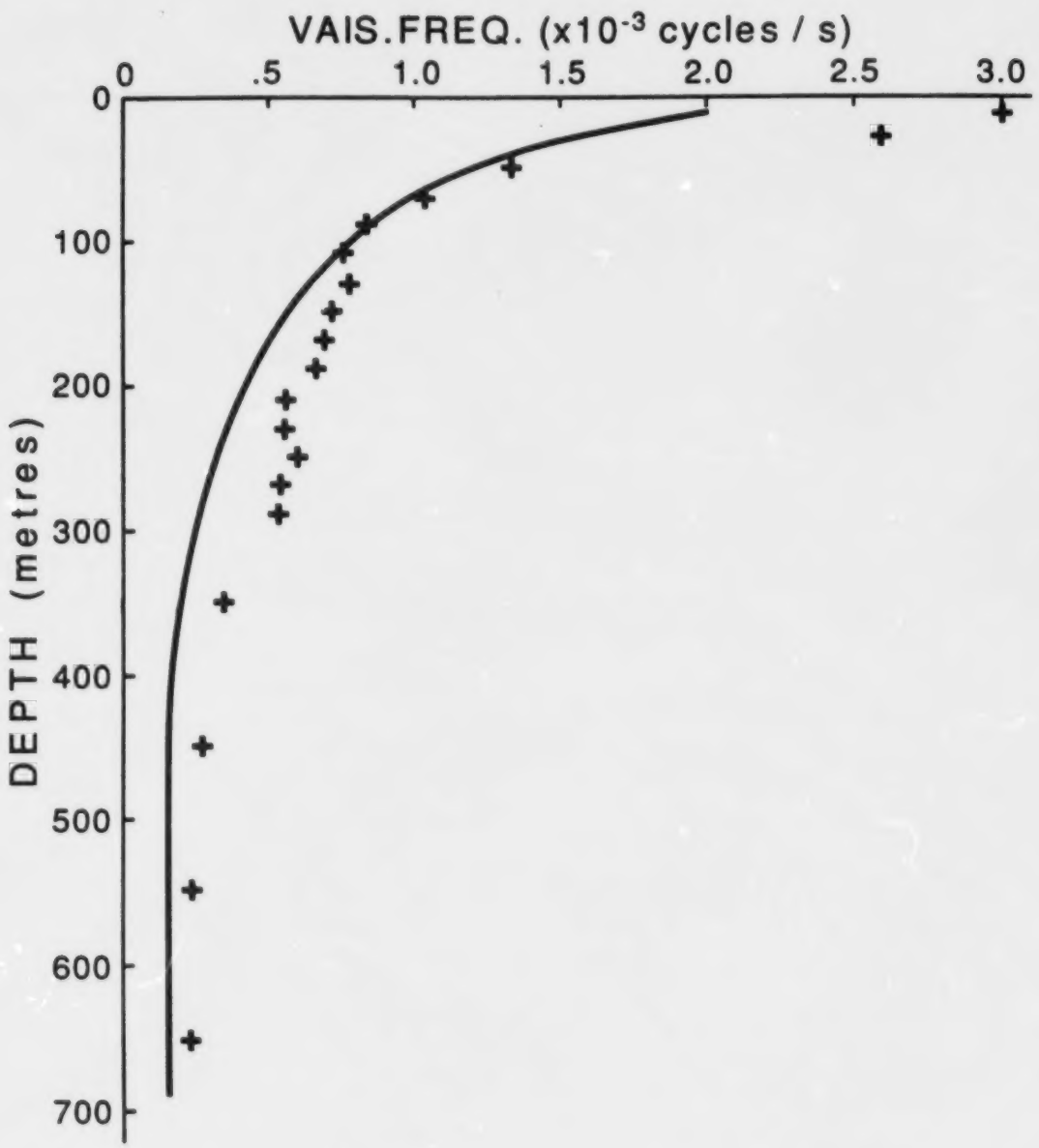

Fig. 8. The buoyancy frequency at the edge of the Labrador shelf. The solid curve denotes a subjective fit to all data collected during the summer of 1980 (Fissel and Lemon, 1982) and the +'s denote averages of estimates obtained during the periods of bottom pressure gauge deployment and retrieval.

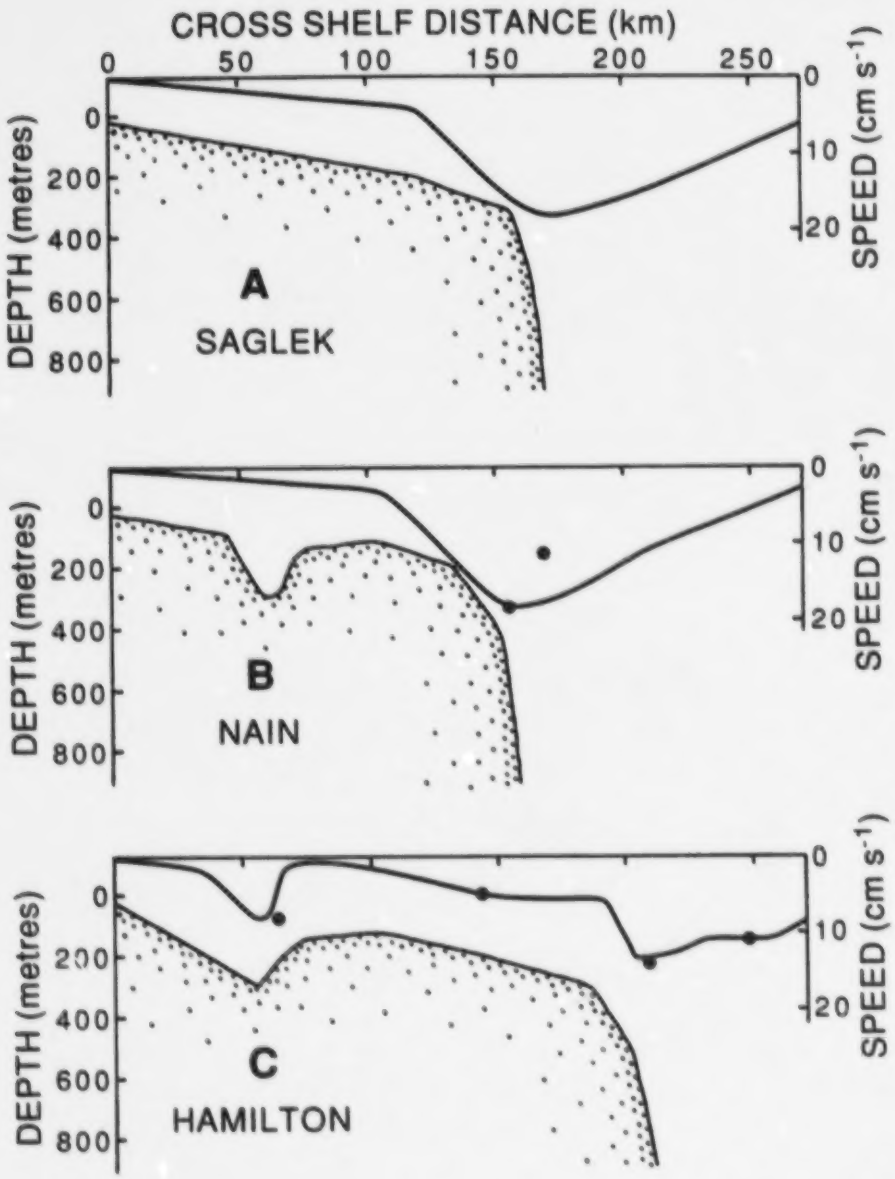

Fig. 9. Cross-shelf bathymetry for (a) Saglek, (b) Nain and (c) Hamilton Banks corresponding to sections (a), (b) and (c) in Fig. 1. The ●'s denote estimates of time and depth averaged observations of longshore current. Broken lines show the actual profiles used in Brink and Chapman's program.

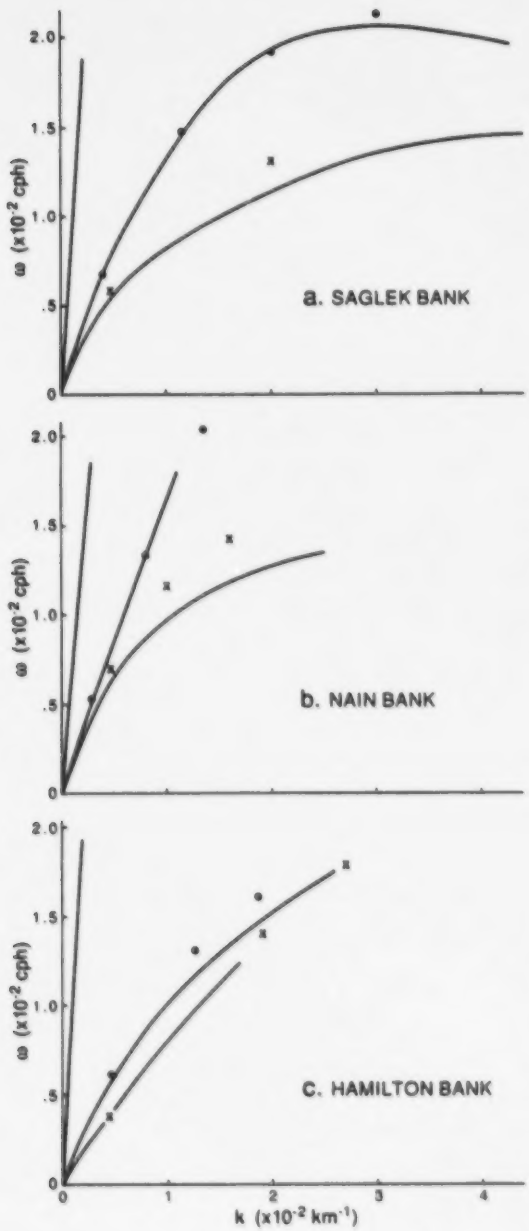

Fig. 10. Dispersion curves for modes 1-3 on (a) Saglek, (b) Nain and (c) Hamilton Banks. The solid curves pertain to a barotropic ocean while the ●'s and ×'s refer to modes 2 and 3 using the estimates of N in Fig. 8. The mode 1 dispersion curves for the barotropic and stratified case are nearly identical.

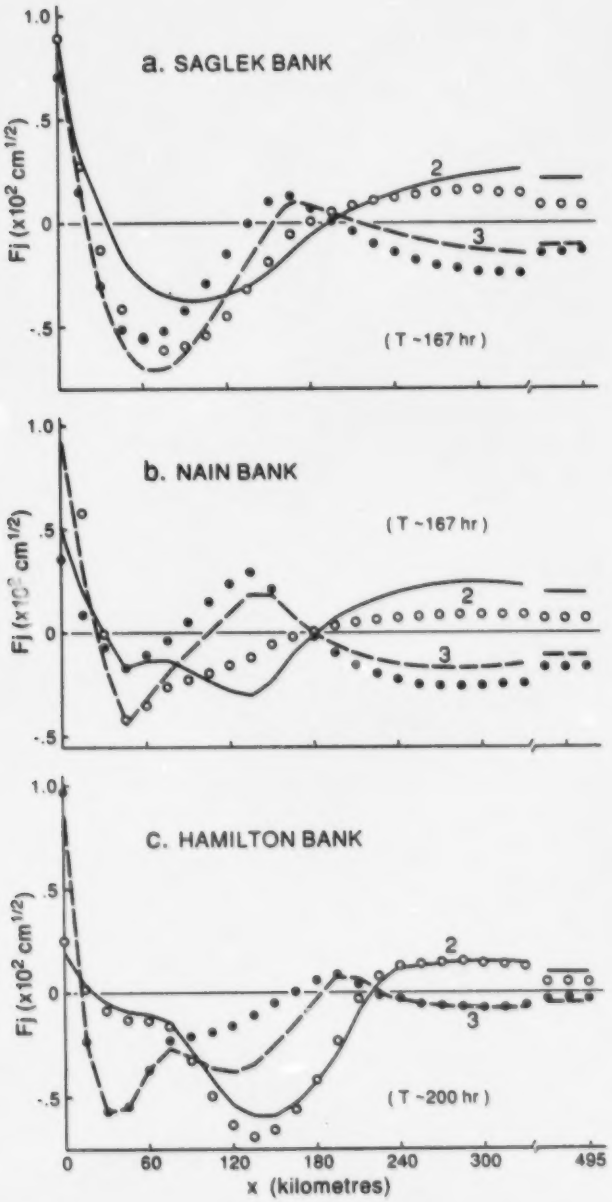

Fig. 11. The low frequency band (period ~167 hr) mode 2 (solid) and 3 (broken) baroclinic eigenfunctions for bottom pressure across (a) Saglek, (b) Nain and (c) Hamilton Banks. The ● and × are the corresponding barotropic estimates. Baroclinic modes were calculated with $u_x = 0$ at x = XMAX while barotropic modes satisfy (3.5). Separated curves at the extreme right of each plot show values at the outer boundary.

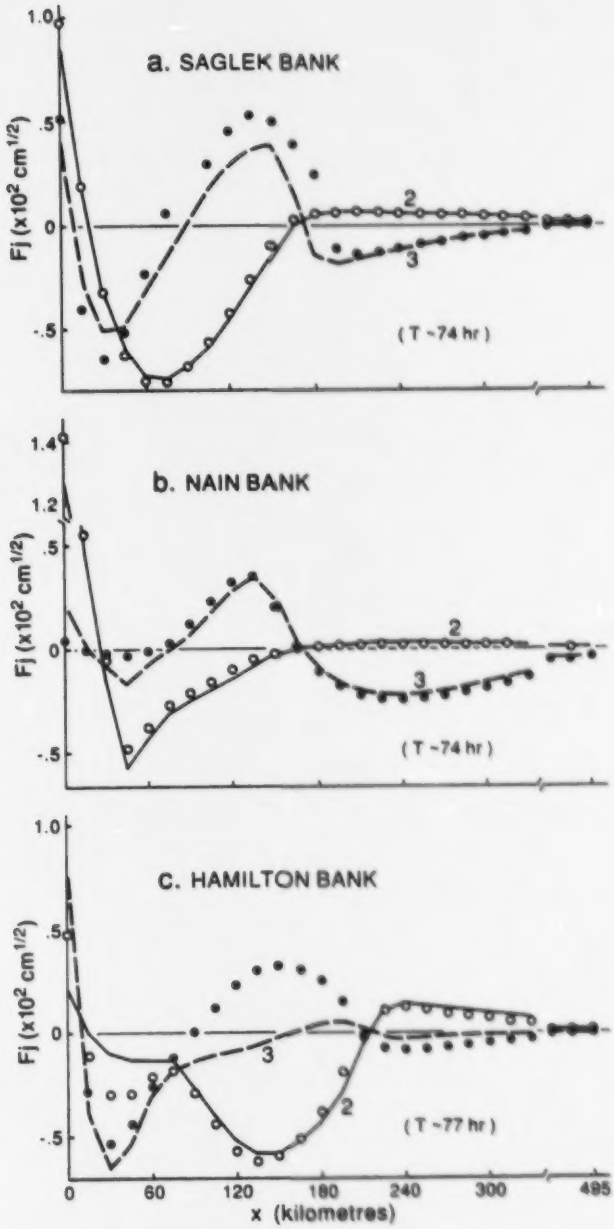

Fig. 12. As in Fig. 11 but for the high frequency band centered around a period of about 3 days.

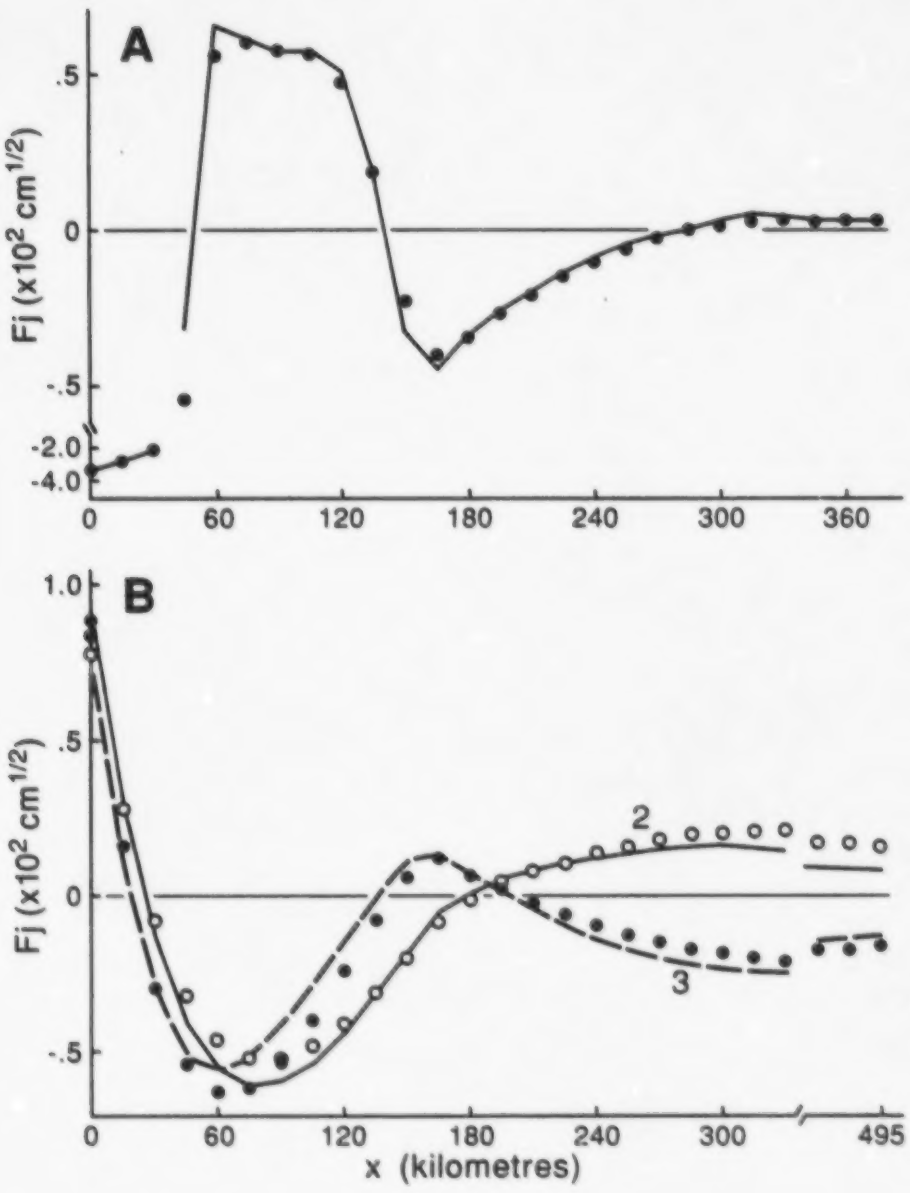

Fig. 13. (a) The longshore velocity at the bottom (solid curve) and surface (+) for mode 3 (stratified) at Nain in the low frequency band (period ≈ 167 hr). (b) The low frequency band (period ≈ 167 hr) barotropic modes 2 and 3. The solid and dashed lines correspond to the condition (3.5) while the ● and x correspond to the condition $u_x = 0$ at x = XMAX.

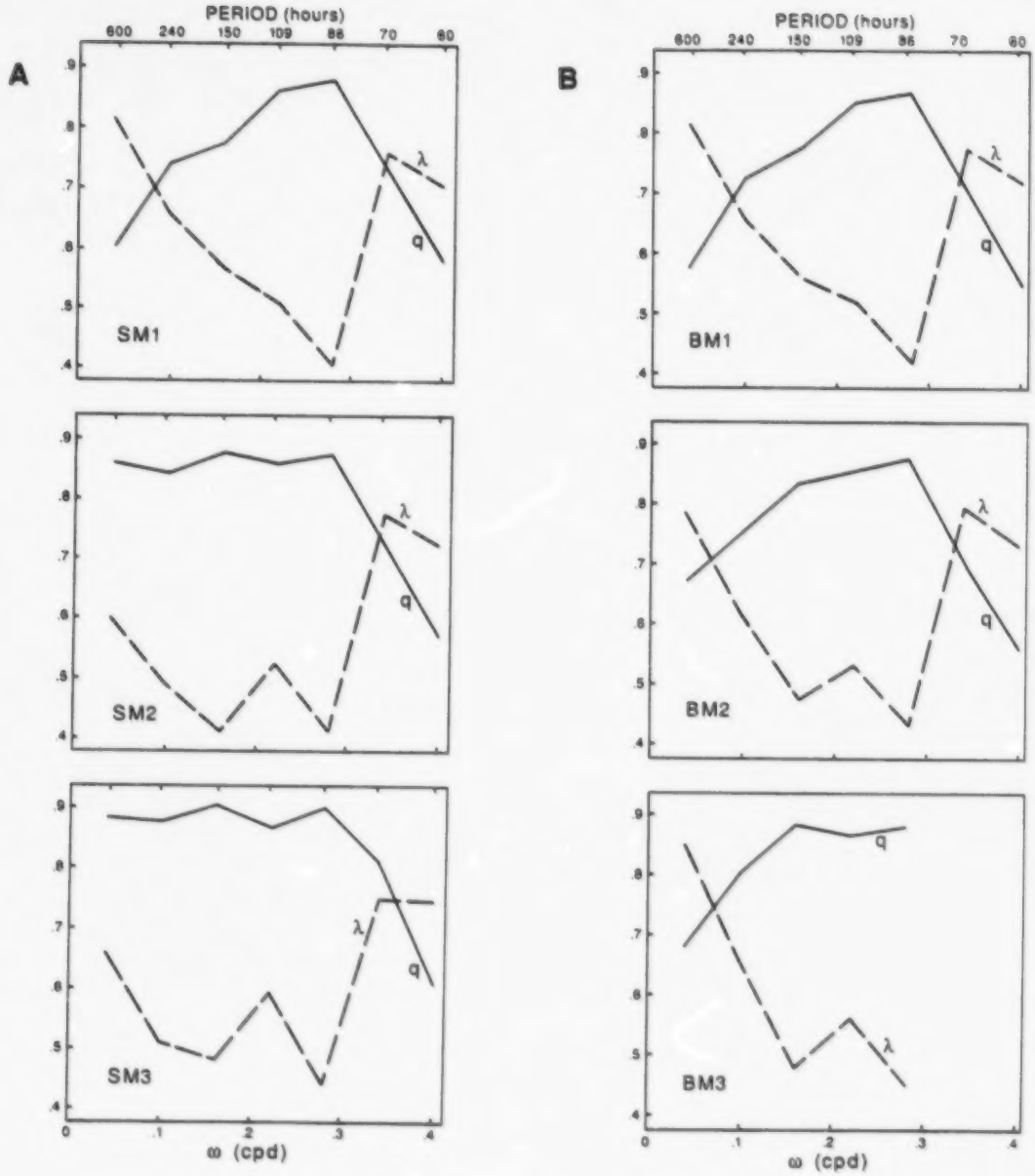

Fig. 14. (a) The explained variance q and largest normalized eigenvalue λ of the residual matrix for the stratified models SM1, SM2 and SM3. For a pure noise residual matrix, $\lambda \leq \lambda_N = 0.28$ at the 95% confidence level.

(b) As for Fig. 14 (a) except for the barotropic models BM1, BM2 and BM3.

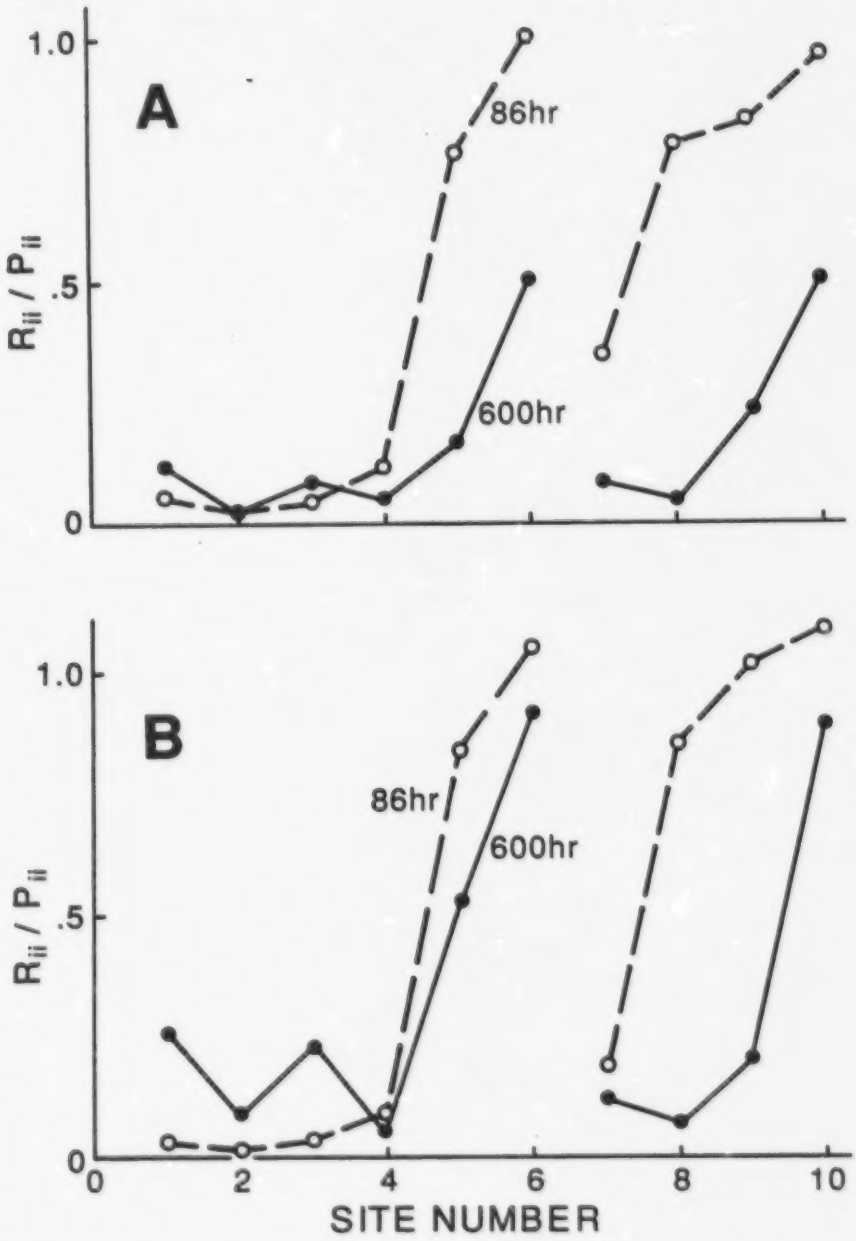

Fig. 15. The normalized residual error $R_{ii}(\omega)/P_{ii}(\omega)$ at each site for the 600 and 86 h bands for (a) model SM2 and (b) model BM2.

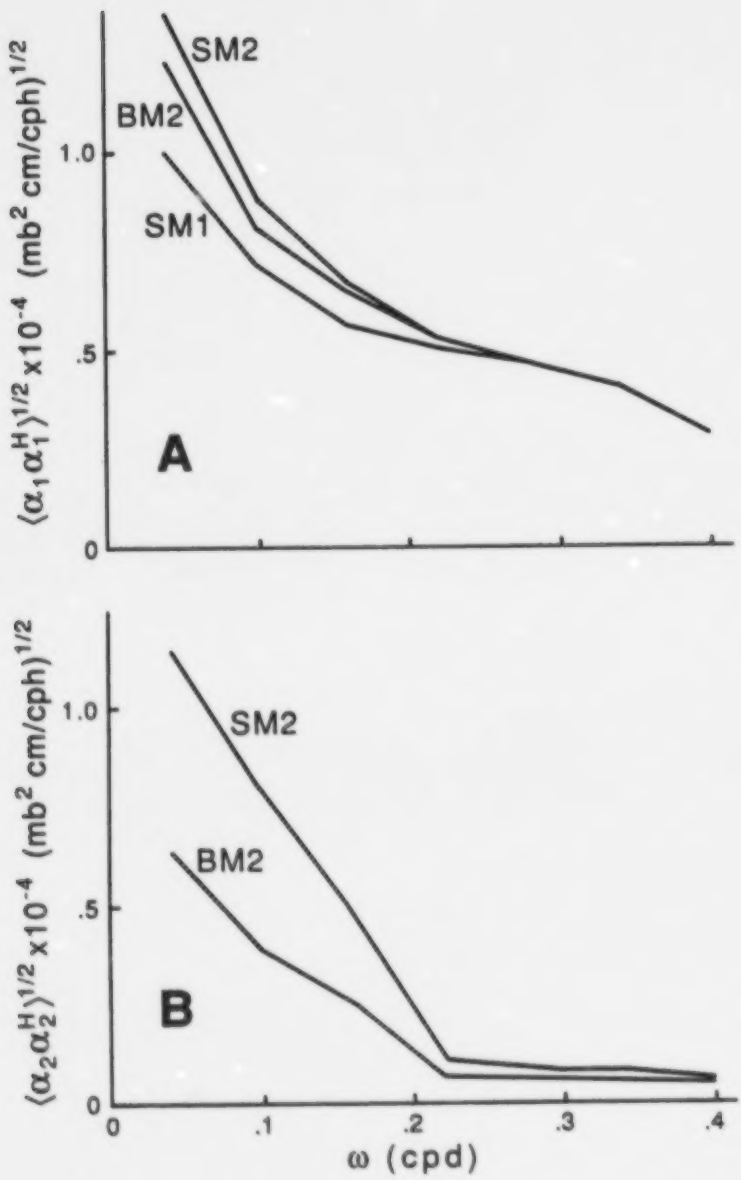

Fig. 16. The fitted modal amplitudes $<\alpha_j \alpha_j^H>^{\frac{1}{2}}$ for (a) mode 1 from models SM1, BM2 and SM2 and (b) mode 2 from models BM2 and SM2.

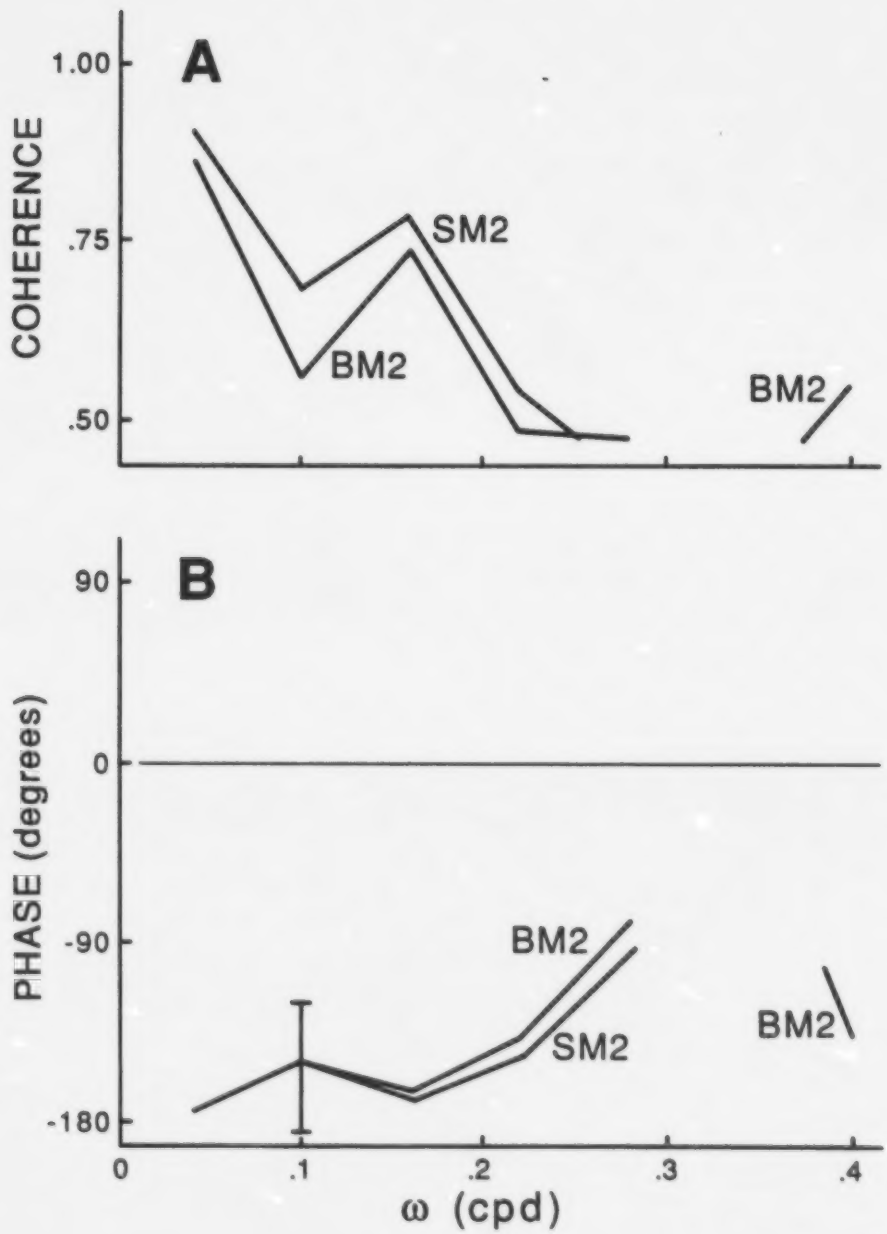

Fig. 17. (a) The coherence (_____) and (b) phase (– –) between modes 1 and 2 for the models SM2 and BM2. Note that a positive phase means mode 1 lags mode 2 and results are only shown for coherences greater than the 95% significance level of 0.48. The confidence intervals for phase are at the 95% level.

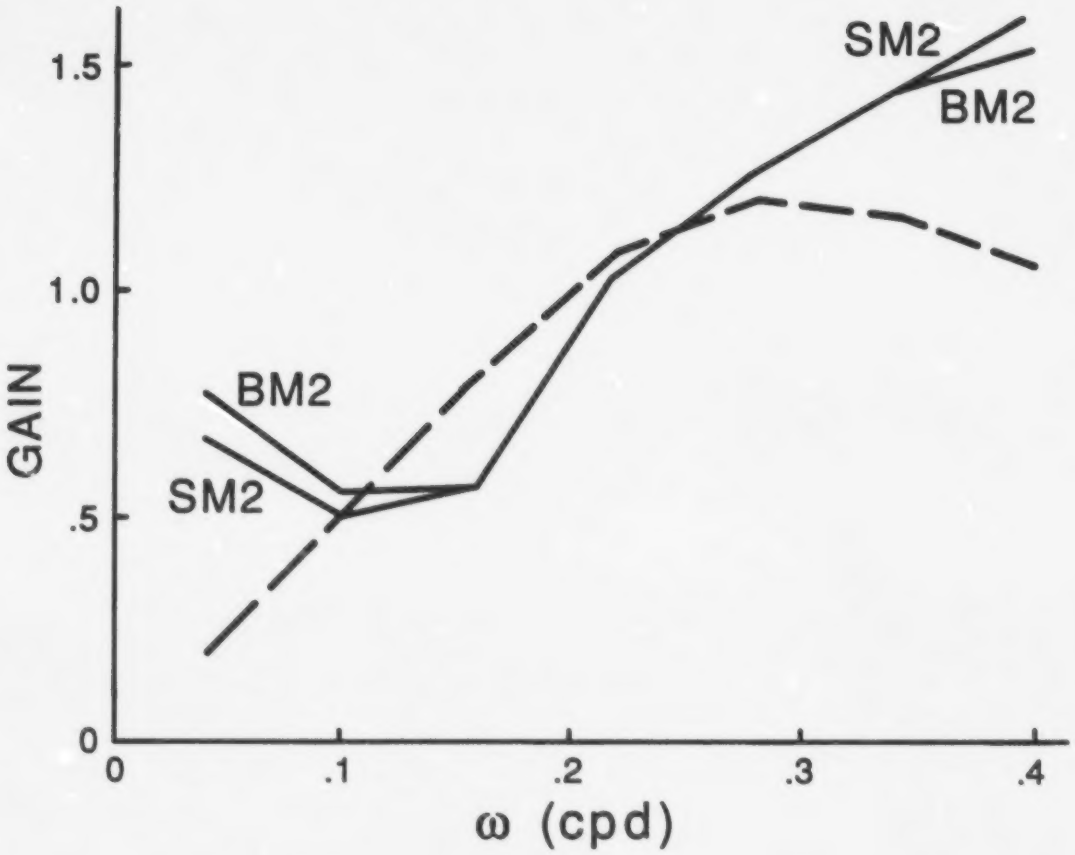

Fig. 18. Gain of model bottom pressure at Cape Chidley with respect to Hudson Bay atmospheric pressure for models SM2 and BM2 (the solid curves). The dashed curve denotes the theoretical response given by Wright *et al.* (1987).

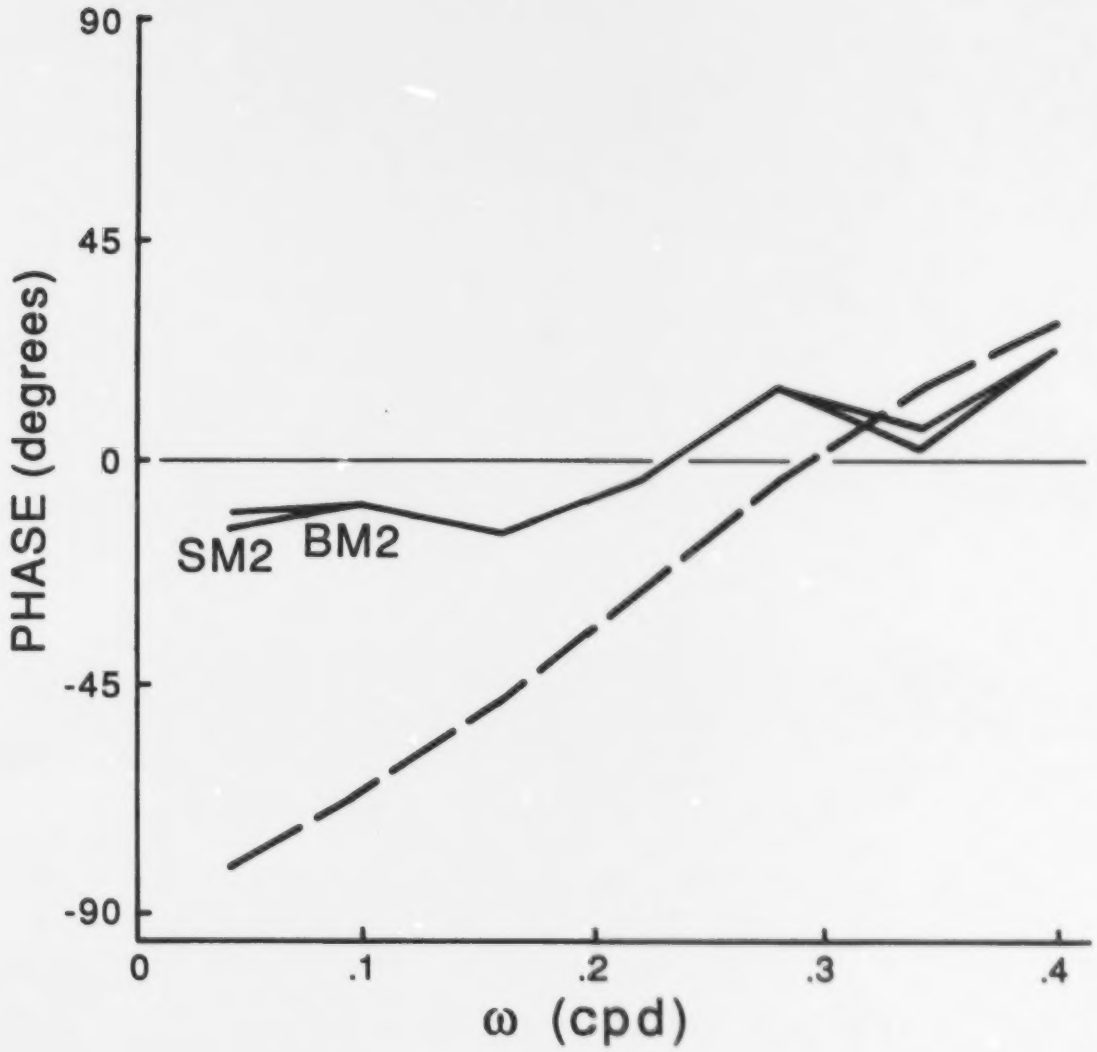

Fig. 19. The phase lag between model bottom pressure at Cape Chidley and Hudson Bay atmospheric pressure for models SM2 and BM2, (the solid curves). The dashed curve denotes the theoretical lag given by Wright *et al.* (1987). A positive phase means bottom pressure lags.

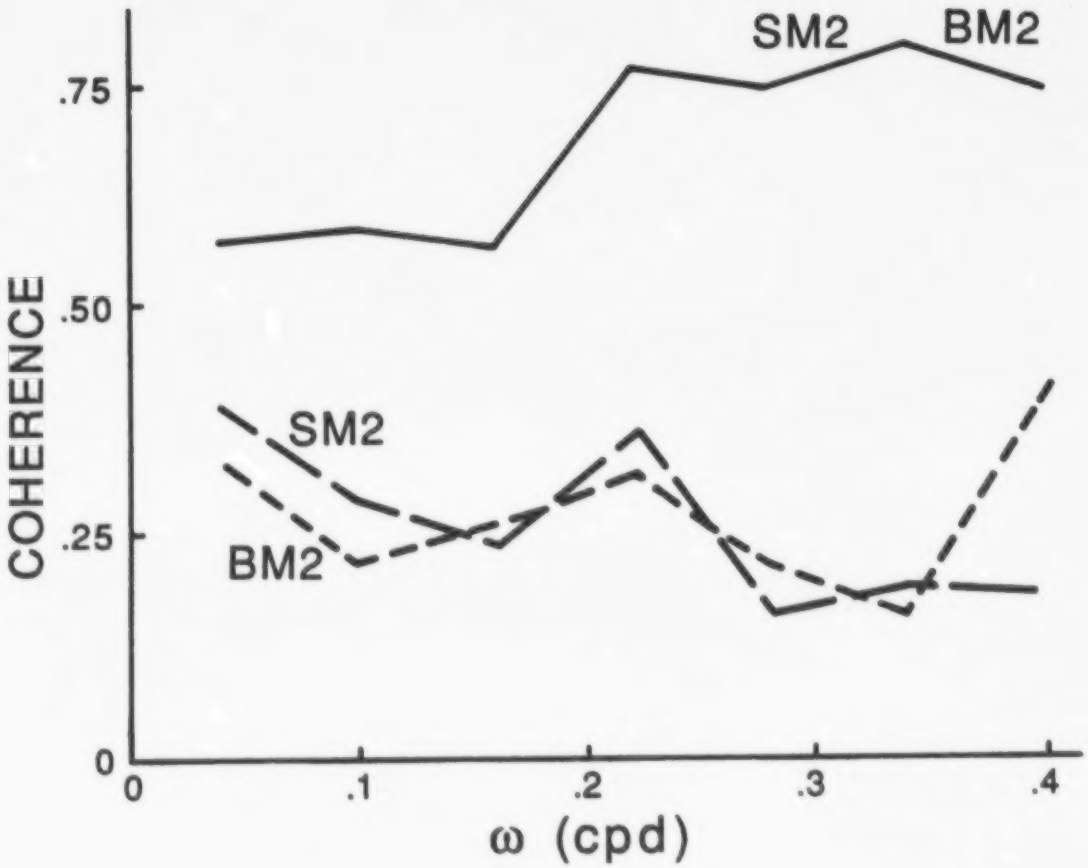

Fig. 20. The coherence between Hudson Bay atmospheric pressure and the amplitude of mode 1 (solid curve) and mode 2 (dashed curve) for models SM2 and BM2. Note the 95% significance level for coherence is 0.48.

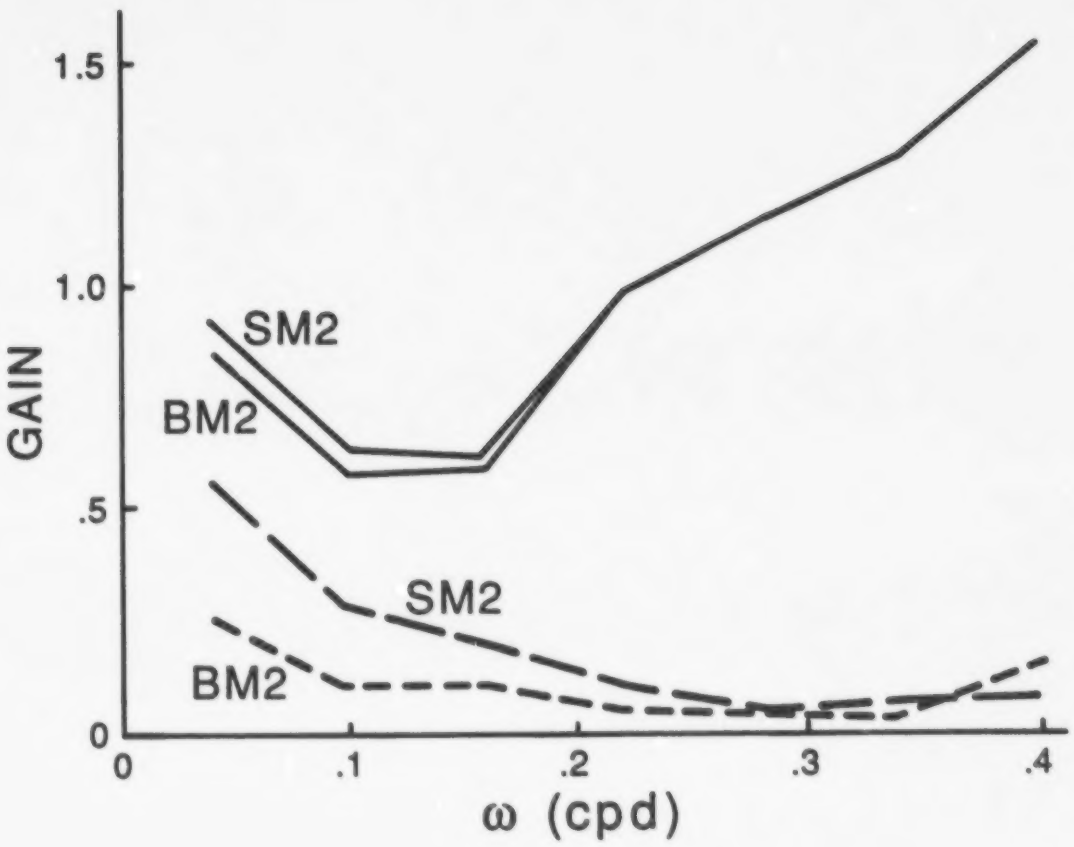

Fig. 21. The gain of mode 1 (solid curve) and mode 2 (dashed curve) with respect to Hudson Bay atmospheric pressure for models SM2 and BM2.

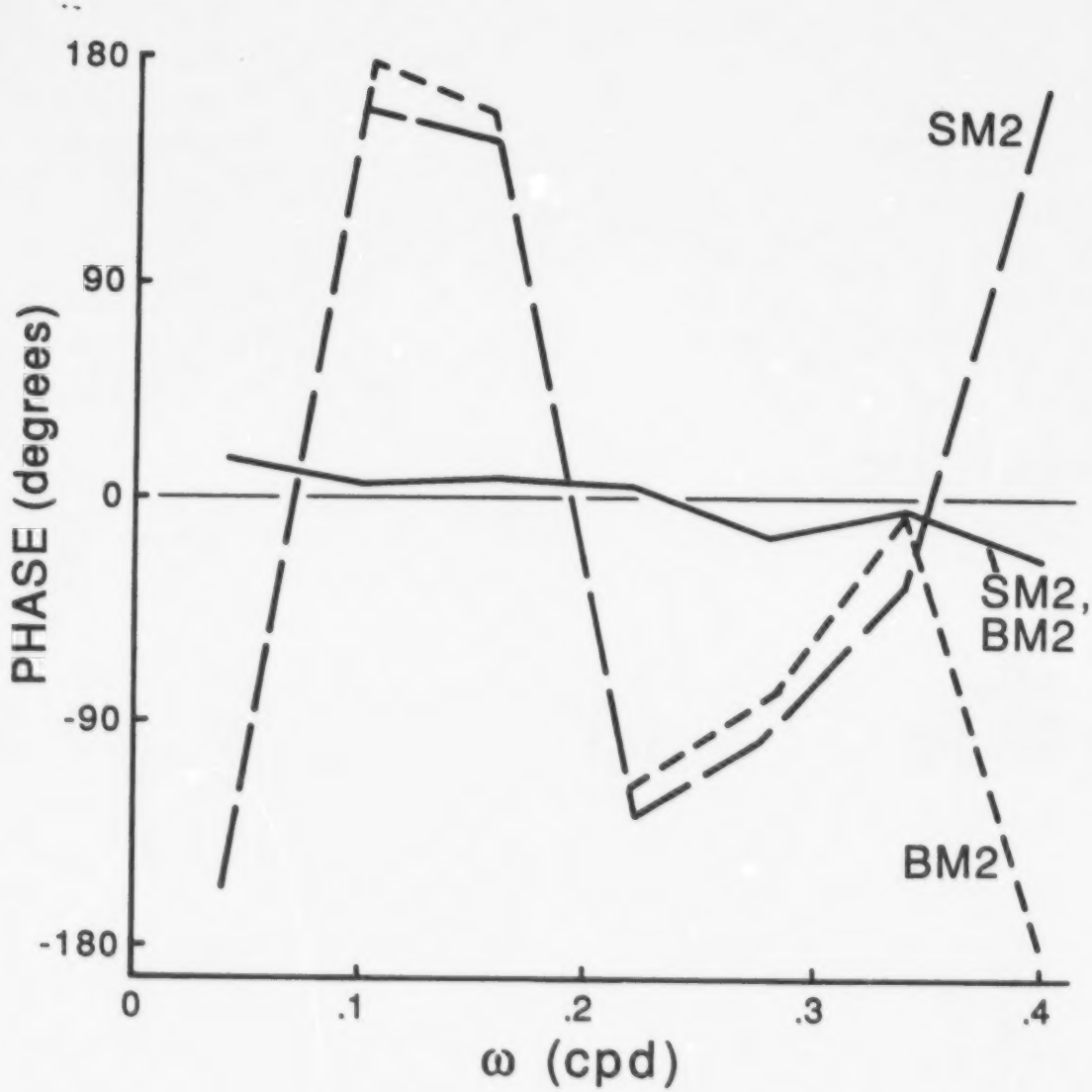

Fig. 22. The phase lag between Hudson Bay atmospheric pressure and mode 1 (solid curve) and mode 2 (dashed curve) for models SM2 and BM2.

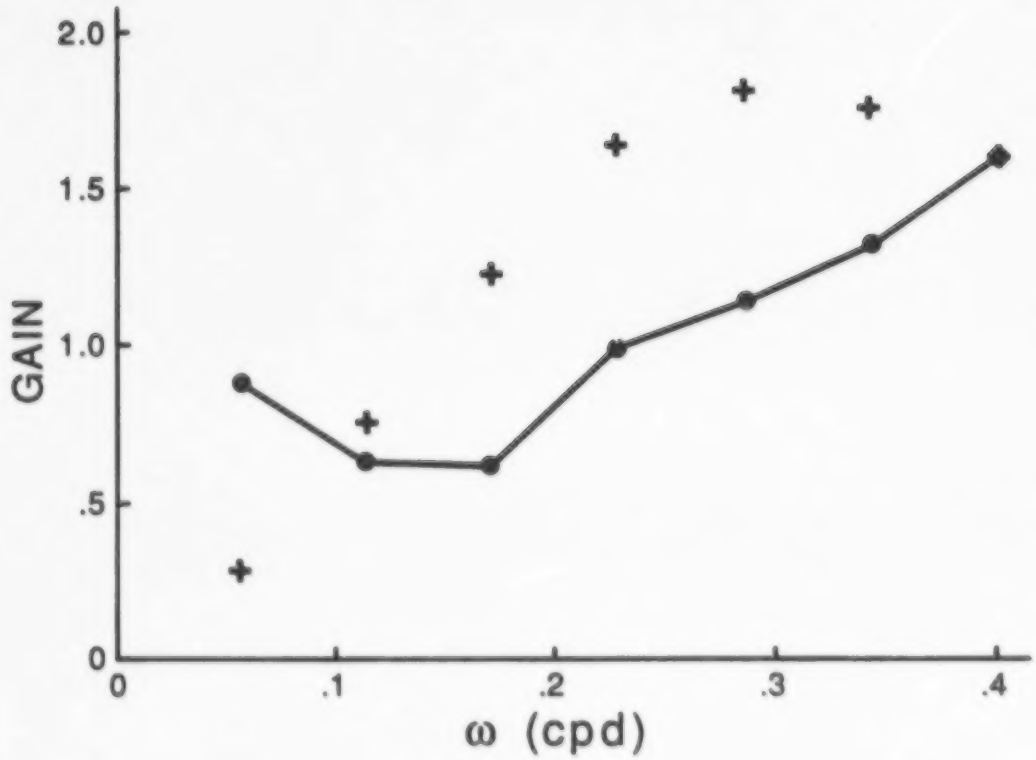

Fig. 23. The gain of mode 1 amplitude with respect to Hudson Bay atmospheric pressure. The solid curve denotes the gain determined from the fit (model SM2) for mode 1 on the shelf proper. The crosses denote the predicted gain of mode 1 amplitude in the region of the strait (Eq. (5.5)).

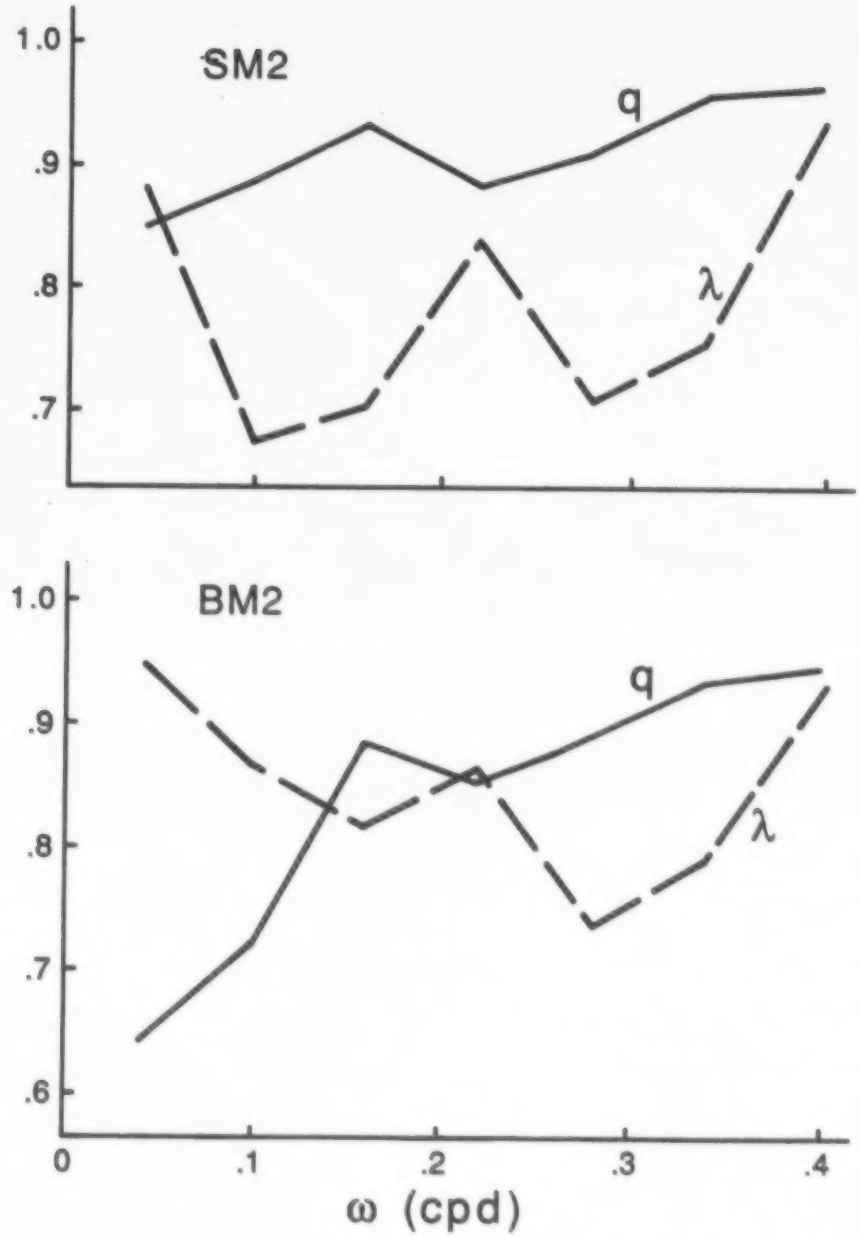

Fig. 24. The explained variance q and eigenvalue λ for the model fit at Nain Bank. For a pure noise residual, $\lambda \leq \lambda_N = 0.49$ at the 95% confidence level.

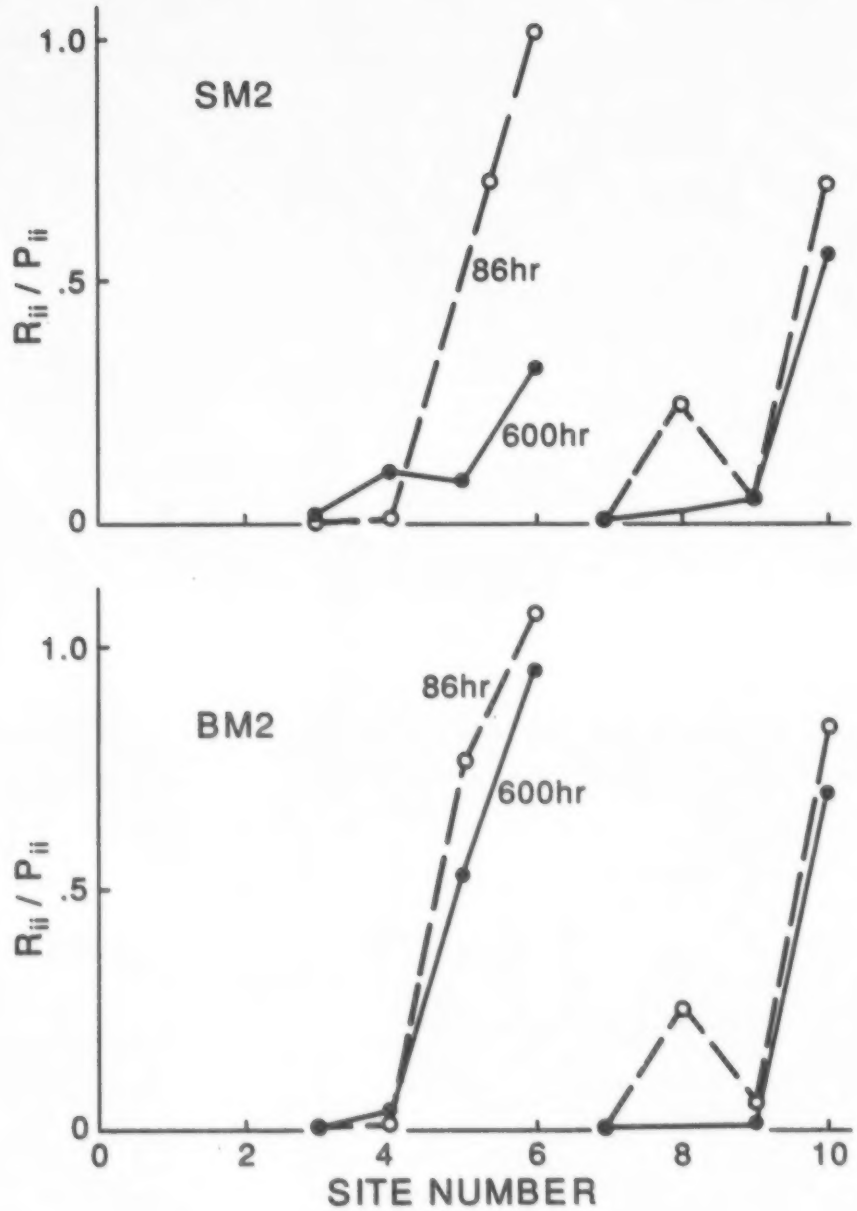

Fig. 25. The normalized residual error $R_{ii}(\omega)/P_{ii}(\omega)$ at each site for the 600 and 86 h bands using models SM2 and BM2. The results shown are for the individual fits at Nain and Hamilton Banks.

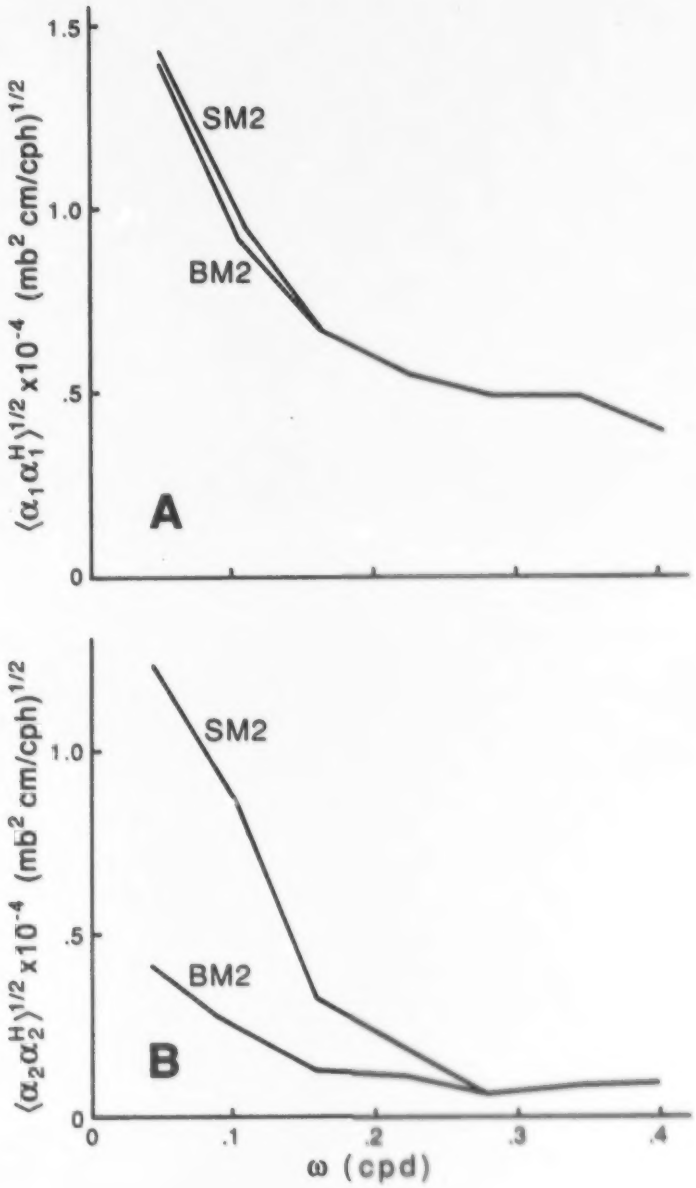

Fig. 26. (a) The fitted mode 1 amplitudes and (b) mode 2 amplitudes using the data at Nain Bank only.

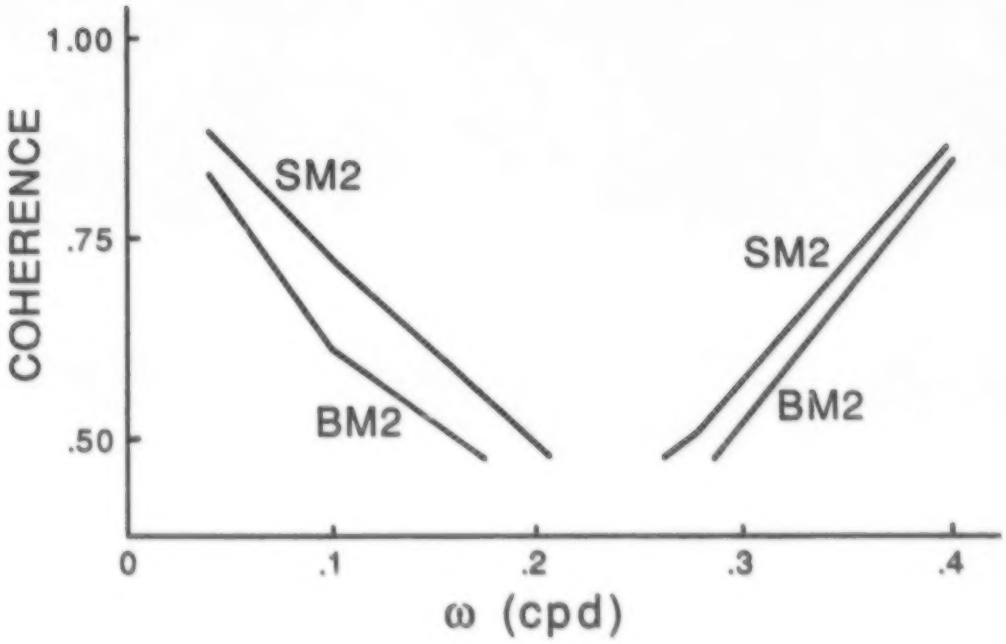

Fig. 27. The coherences between modes 1 and 2 for the model fit at Nain Bank.

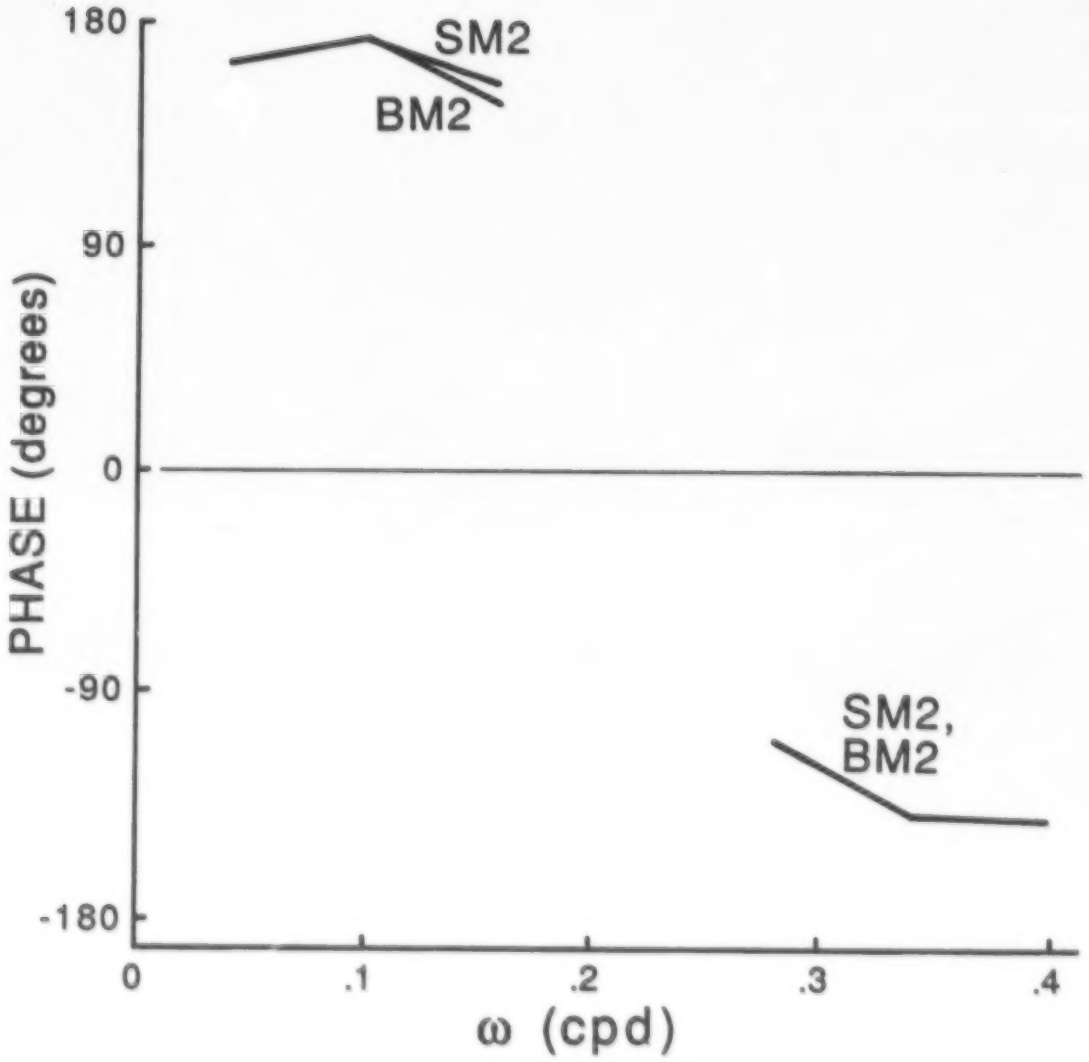

Fig. 28. The phase between modes 1 and 2 for the model fit at Nain Bank. A positive phase means mode 1 lags.

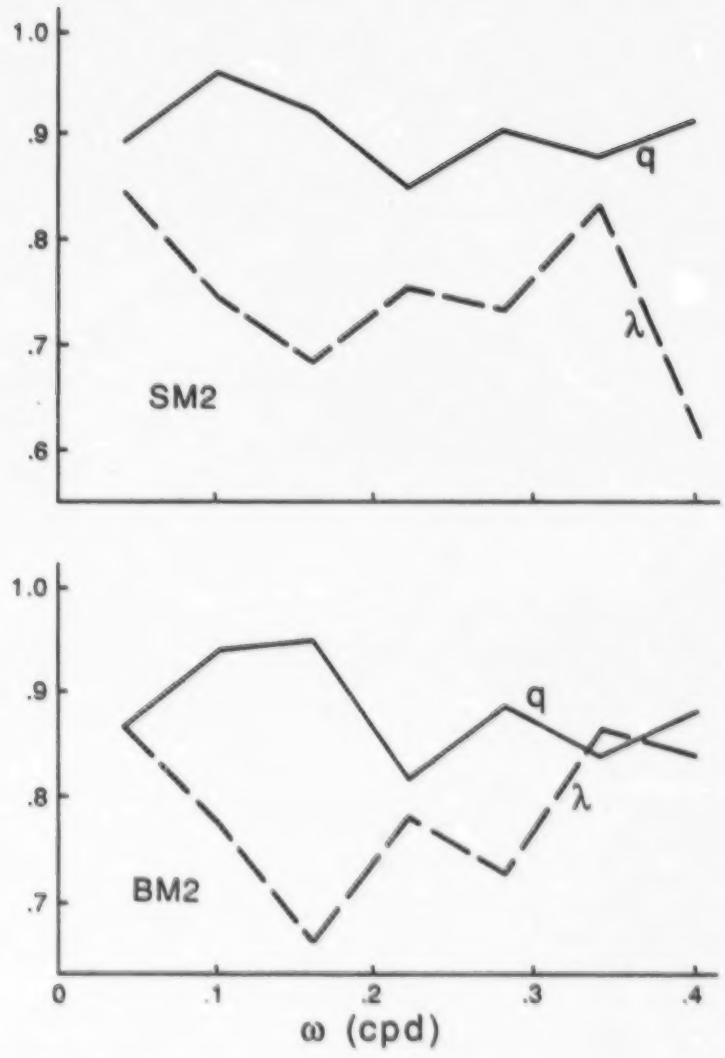

Fig. 29. The explained variance q and eigenvalue λ for the model fit at Hamilton Bank.

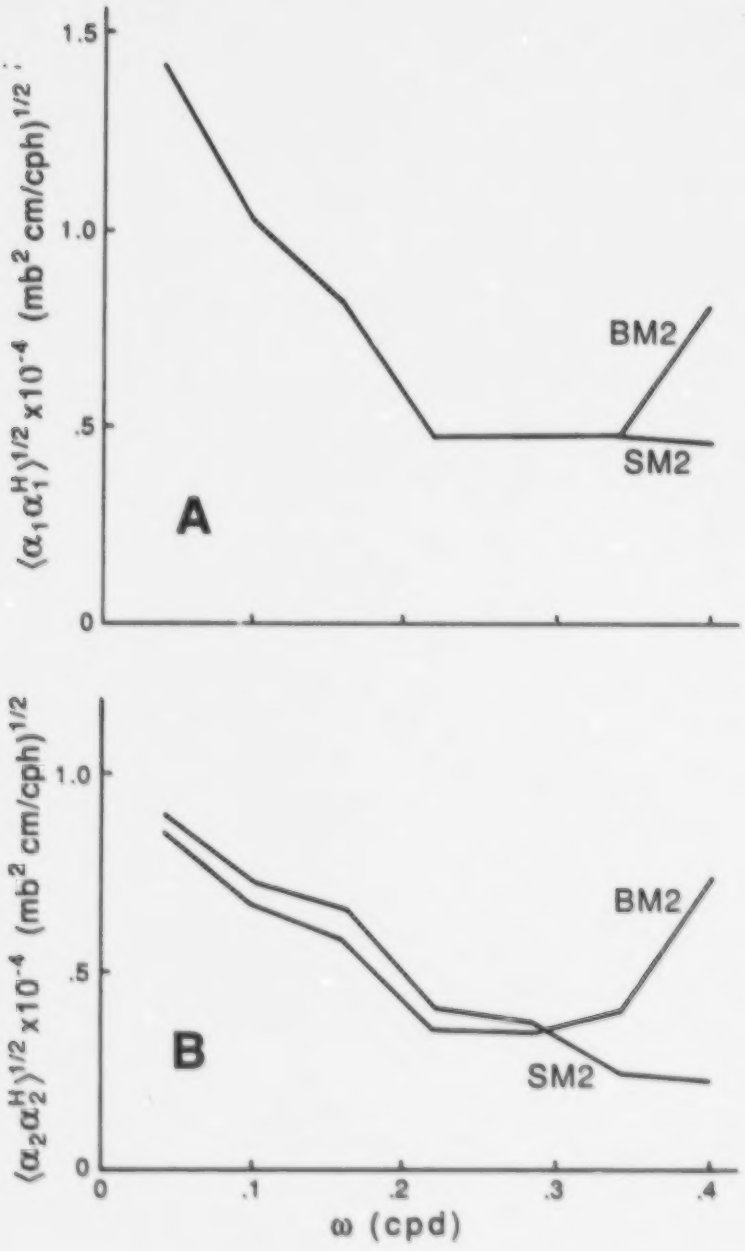

Fig. 30. (a) The fitted mode 1 amplitudes and (b) the mode 2 amplitudes using the data at Hamilton Bank only.

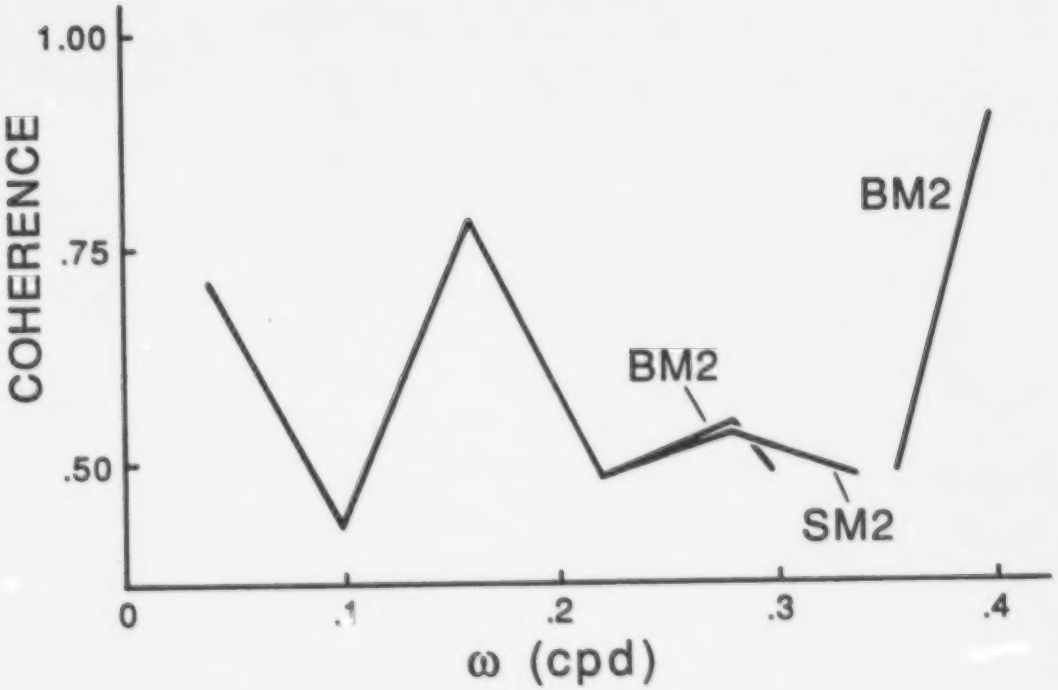

Fig. 31. The coherences between modes 1 and 2 for the model fit at Hamilton Bank.

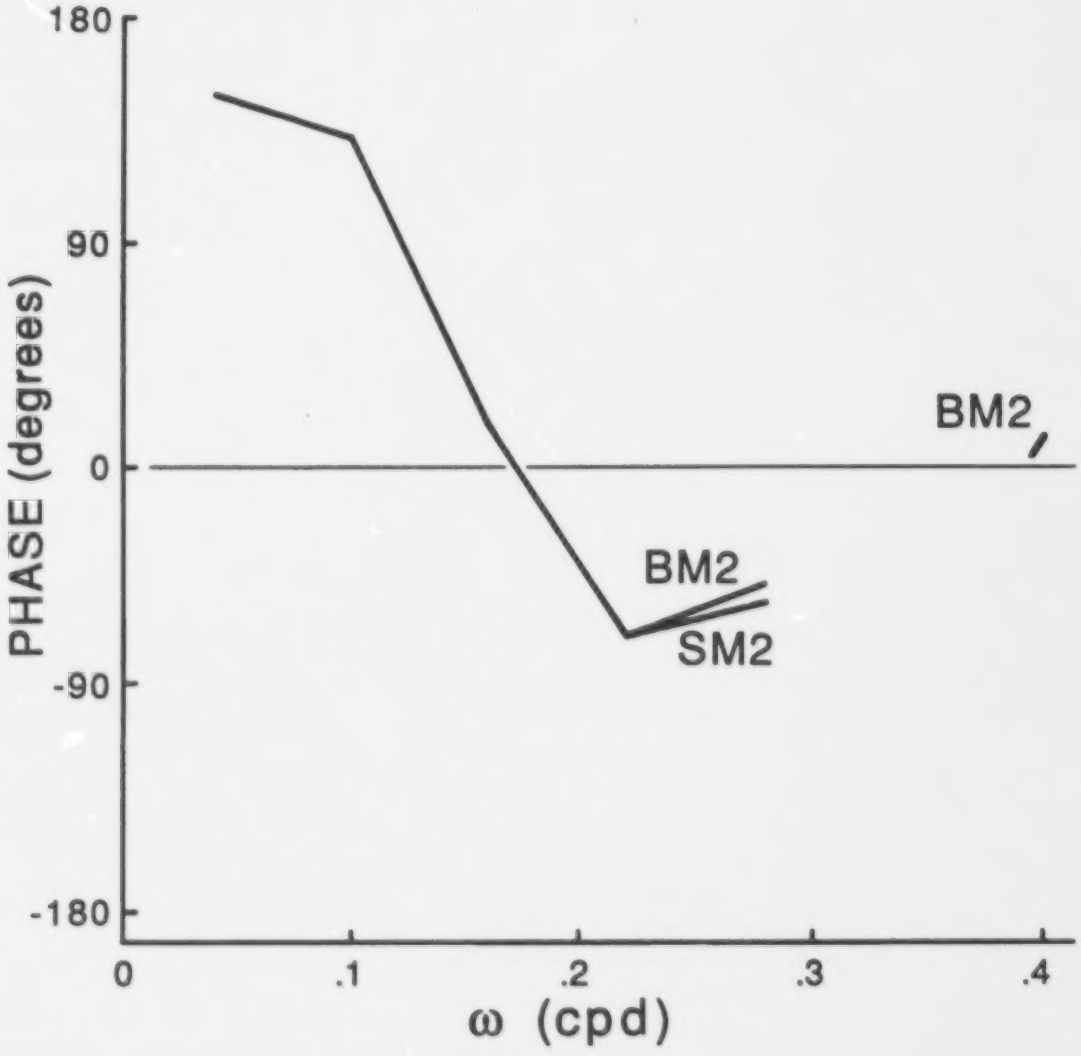

Fig. 32. The phase lag between modes 1 and 2 for the model fit at Hamilton Bank. A positive phase means mode 1 lags.